

Accounts

Roles of Molecular Wires between Fullerenes and Electron Donors in Photoinduced Electron Transfer

Osamu Ito[*,†] **and Ken-ichi Yamanaka**[††]

Institute of Multidisciplinary Research for Advanced Materials, Tohoku University, Katahira, Aoba-ku, Sendai 980-8577

Received August 1, 2008; E-mail: ito@tagen.tohoku.ac.jp

In the photoinduced intramolecular electron transfer events of donor–bridge–acceptor molecular systems, the bridges play important roles. In the first part of this account, we review charge separation and charge recombination of porphyrin–bridge–fullerene systems, in which the porphyrin acts as a photosensitizing electron donor, whereas the ground state of the C_{60} moiety acts as an electron acceptor. In such systems, the charge separation usually takes place through the LUMO of the bridges via a super-exchange mechanism and/or a hopping mechanism, depending on their relative LUMO energy levels. On the other hand, the charge recombination of the radical ion pairs usually takes place through the HOMO of the bridges. In the second part, research of charge separation via the excited state of fullerene through the HOMO of the bridges is reviewed. So far, very small damping factors have been reported for π-conjugated bridges such as oligophenyleneacetylenes, oligothiophenes, and oligothiophenevinylenes. On summarizing these results, it is revealed that switching from the super-exchange mechanism in short bridges to hopping mechanism in longer bridges is important to achieve long distance electron transfer through the bridges.

Photoinduced electron transfer (ET) of donor–acceptor systems is the most elementary of all photochemical reactions, and plays a crucial role in many essential photoactive devices.[1–4] The functions of conjugated nano-scale donor–acceptor molecules are useful for molecular electronic devices[5] and photovoltaic cells.[6,7] Photo-induced electron-transfer systems exhibiting charge-separation (CS) and charge-recombination (CR) processes of the covalently connected donor–spacer–acceptor systems, in which the spacers are flexible methylene chains, have been extensively studied by the Okada, Mataga, Sakata, and Misumi groups.[8–11] Recently, fullerene derivatives have been widely applied to construct photovoltaic cells.[12,13] For further advances of these chemically modified fullerenes as molecular electronic devices, it is very important to reveal the general roles of the bridges in the covalently connected donor–bridge–acceptor (D–B–A) systems, in which the donor and acceptor can be photo-excited as illustrated in Figure 1.[14]

When the D moiety in a D–B–A system is photo-excited, the excited state of D (D^*) acts as a photosensitizing electron donor, thus CS takes place from D^* to the A moiety through the LUMO of B, giving finally the radical ion pair $D^{\bullet+}$–B–$A^{\bullet-}$ as illustrated in Figure 2. In this photosensitizing CS process via D^*, two cases can be considered depending on the energy

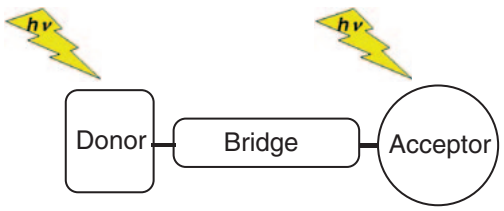

Figure 1. Covalently connected donor–bridge–acceptor (D–B–A) molecular systems.

level of the LUMO of the B unit relative to the LUMO level of D. One is super-exchange, in which the LUMO energy level of B is higher than the LUMO levels of D and A and another is electron hopping, in which the LUMO level of B is lower than the LUMO level of D.[15,16] Thus, in the super-exchange mechanism, the first-step CS (CS-1) after initial photo-excitation (CS-0) is endothermic and the second-step CS (CS-2) is exothermic as shown in Figure 2.

For the CR of $D^{\bullet+}$–B–$A^{\bullet-}$ after CS via super-exchange, one possible process is endothermic electron transfer from the HOMO of B to the half-vacant HOMO of $D^{\bullet+}$ as shown in CR-1 in Figure 3. The electron of the half-filled LUMO of $A^{\bullet-}$ then exothermically falls to the half-vacant HOMO of the transient $B^{\bullet+}$ (CR-2), returning to the original neutral molecule in the ground state. Another possible process after super-exchange CS is a jump of an electron from the half-filled LUMO of $A^{\bullet-}$ up to the vacant LUMO of B (CR-1′), from

† Present address: Institute of CarbonPhotoScience, 2-1-1 Kita-Nakayama, Izumi-ku, Sendai 981-3215

†† Present address: Toyota Central R&D Laboratories, Inc., Nagakute, Aichi-gun, Aichi 480-1192

Published on the web March 12, 2009; doi:10.1246/bcsj.82.316

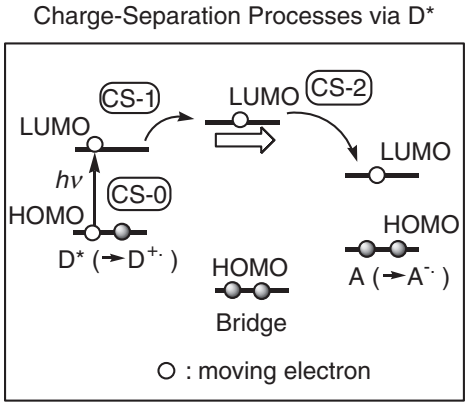

Figure 2. Schematic illustration of photo-induced CS via D* in D–B–A molecular system.

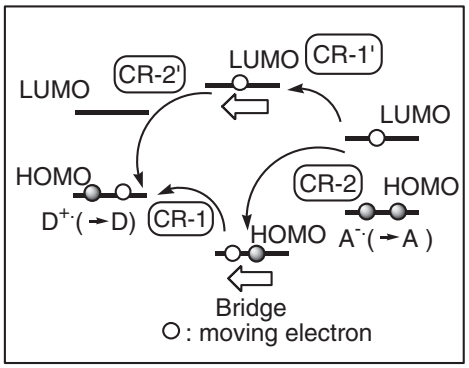

Figure 3. Schematic illustration of photo-induced CR from $D^{\bullet+}$–B–$A^{\bullet-}$.

which the electron falls down to the half-vacant HOMO of $D^{\bullet+}$ (CR-2′). One of two CR routes can be selected by the comparison of the energy barriers of CR-1 with that of CR-1′ in Figure 3.

On the other hand, the CS via electron-hopping takes place when the LUMO energy level of the B unit is lower than the LUMO level of D. Since the LUMO level of A is usually lower than the LUMO level of B, both the CS-1 and CS-2 processes must be exothermic after photo-excitation of D. For the CR of $D^{\bullet+}$–B–$A^{\bullet-}$ after electron hopping, the electron transfer from the HOMO of B to the half-vacant HOMO of $D^{\bullet+}$ takes place exothermically when the HOMO energy level of B is higher than the half-vacant HOMO energy level of $D^{\bullet+}$. The electron of the half-filled LUMO of $A^{\bullet-}$ then falls to the half-vacant HOMO of transient $B^{\bullet+}$, returning to the starting neutral molecule in the ground state. Since the energy level of the LUMO of B may be near the energy level of the half-filled LUMO of $A^{\bullet-}$, CR from the half-filled LUMO of $A^{\bullet-}$ to the LUMO of B (CR-1′) and successive electron transfer to the half-vacant HOMO of $D^{\bullet+}$ (CR-2′) may also take place easily.

When the A moiety in a D–B–A system acts as a photo-sensitizing electron acceptor, CS takes place initially from the HOMO of B to the half-vacant HOMO of A* (CS-1). Then, an electron in the HOMO of D migrates to the half-vacant HOMO of B (CS-2) as illustrated in Figure 4. In this case, the LUMOs

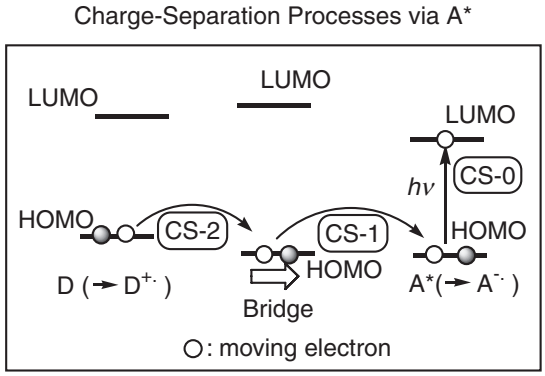

Figure 4. Schematic illustration of photo-induced CS of via A*.

of B and D do not play any role. When the energy level of the HOMO of B is lower than the half-vacant HOMO of A*, CS-1 is endothermic, whereas CS-2 becomes exothermic. When the energy level of the HOMO of B is higher than that of the half-vacant HOMO of A*, CS-1 becomes exothermic. On the other hand, CS-2 becomes endothermic, which corresponds to electron hopping. For the CR process, two routes are possible similar to the schemes shown in Figure 3.

In order to evaluate the electron-transfer ability through the bridges, a damping factor (β_{ET}) is defined as eq 1;[15,16]

$$\ln k_{ET} = \ln k^0_{ET} - \beta_{ET} R_{CC} \quad (1)$$

where k_{ET} is referred to as the rate constant of electron transfer between D and A through a bridge with length R_{CC} and k^0_{ET} for $R_{CC} = 0$. Small β_{ET} implies long-distance electron-transfer ability through the bridges. For example, for $\beta_{ET} = 0.23\,Å^{-1}$, $k_{ET}/k^0_{ET} = 1/10$ at $R_{CC} = 10\,Å$ ($Å = 10^{-10}\,m$). For smaller β_{ET} value, i.e., $\beta_{ET} = 0.023\,Å^{-1}$, $k_{ET}/k^0_{ET} = 1/10$ at $R_{CC} = 100\,Å$. However, in photo-induced CS, an upper limit of long distant CS is present depending on the lifetimes of the excited state of the photo-sensitizers, because the CS process competes with the lifetimes of the excited state of the photosensitizing donor or acceptor. For example, when the lifetime of the singlet photo-excited state of the donor or acceptor is $10^9\,s^{-1}$, CS at 20 Å takes place only about 50% for $k^0_{ET} = 10^{10}\,s^{-1}$ and $\beta_{ET} = 0.23\,Å^{-1}$, competing with the deactivation of the excited state such as intersystem crossing (ISC).

Prophyrin Excitation of Porphyrin–Bridge–Fullerene Molecules

The most frequently studied D–B–A systems in recent years have been porphyrin–bridge–fullerene molecular systems (MP–B–C_{60}, in which M = H_2, Zn, and Mg in Figure 5), since the MPs are typical photo-sensitizing electron donors as a model of chlorophylls involved in the early events of photo-synthesis.[17–19] Fullerene (C_{60}) has been employed as an excellent electron acceptor, because of the high electron affinity and stability of the C_{60} radical anion ($C_{60}^{\bullet-}$) in addition to its small reorganization energy.[20–22] In supramolecular systems, the MP derivatives also act as light-harvesting antenna molecules in addition to photosensitizing electron donors vs. chemically modified C_{60}.[23]

Various linkage modes to connect the MP moiety to

fullerene are known. The bridging points of the MP and C_{60} to the ends of B are important to control the first steps such as CS-1 and CR-1, which strongly affect the efficiency and rates of photo-induced CS and subsequent CR, in addition to the relative energy levels of the LUMOs and HOMOs.

As an example of the shortest bridge, compound **1** is shown in Figure 6;[24,25] in which only three saturated bonds are used to connect one of the phenyl rings of ZnP with the fullerene π-systems. In this case, the CS rate constant (k^S_{CS}) via the singlet excited state of the ZnP moiety (^{1}ZnP*) was evaluated from the accelerated decay of the $S_n \leftarrow S_1$ absorption bands of ZnP by the attached C_{60} in pico-second transient absorption spectra.[24,25] The k^S_{CS} values were also evaluated from the observed shortening of the fluorescence lifetimes of ^{1}ZnP* in the ZnP–B–C_{60} dyads as compared with the pristine ^{1}ZnP* as shown in the fluorescence time-profiles at 625 nm in Figure 7.[27] The discrimination of CS from the energy transfer (EnT) from ^{1}MP* to C_{60} has been usually judged by solvent effects in fluorescence time-profile measurements. In polar solvents, CS is accelerated, whereas the EnT rate is usually invariant with changes in solvent polarity. In addition, the EnT of the singlet excited state of the ZnP–C_{60} dyads can be confirmed by the appearance of new fluorescence due to the C_{60} near 720 nm, which is frequently observed only in non-polar solvents.[28] The k^S_{CS} value via ^{1}ZnP* was evaluated to be fast at 4×10^{10} s^{-1} in benzonitrile (PhCN) at room temperature (RT).[24,25] On inserting an amide bond between the ZnP and C_{60} moieties (compound **2** in Figure 6),[26] the k^S_{CS} value was estimated to be ca. 1×10^{10} s^{-1}, which is considerably smaller than that of compound **1**. Since the LUMO levels of the single bonds are quite higher than those of ZnP, CS of these two cases may belong to the super-exchange mechanism (Figure 2), which is effective in short range CS between highly π-systems such as an excited MP and a C_{60}. As for the CR of ZnP$^{\bullet+}$–B–$C_{60}^{\bullet-}$ after CS, a two-step mechanism was reported.[26,29] That is, fast CR via ZnP$^{\bullet+}$–B–$C_{60}^{\bullet-}$ in a singlet spin state, which is referred as to k^S_{CR}, takes place, then successive slow CR via ZnP$^{\bullet+}$–B–$C_{60}^{\bullet-}$ in a triplet state, which is referred as to k^T_{CR}, occurs. The former process can be followed by pico-second transient absorption spectra and was determined to be k^S_{CR} = ca. 1×10^9 s^{-1} at RT.[26] In addition, a slow increase of $C_{60}^{\bullet-}$ was observed at 1000 nm as shown in the nano-second transition absorption spectra in Figure 8.[26] From the increase of $C_{60}^{\bullet-}$, the rates of CS via the triplet excited state of the C_{60} are determined to be ca. 1×10^7 s^{-1} at RT.[26] Rates of such slow increases of the radical ion pair in the CS-state are in good agreement with the decay of the triplet state of the components such as $^3C_{60}$* at 700 nm.[26,28] This observation indicates that rapid CR from ZnP$^{\bullet+}$–B–$C_{60}^{\bullet-}$ with a singlet spin generates the $^3C_{60}$*, from which the ZnP$^{\bullet+}$–B–$C_{60}^{\bullet-}$ in a triplet spin state

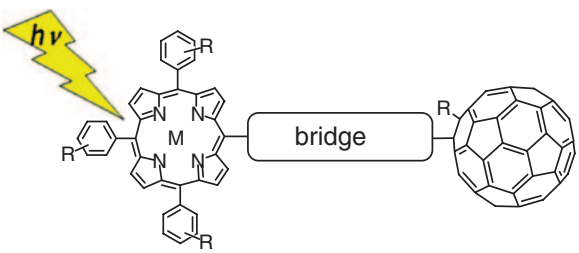

Figure 5. A typical porphyrin–bridge–fullerene molecular system (MP–B–C_{60}; M referrers to central metal).

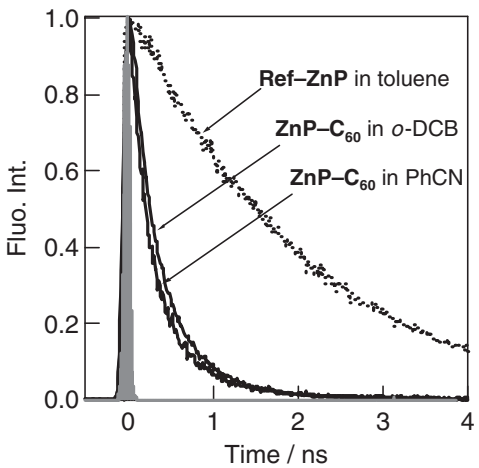

Figure 7. Time profiles of fluorescence at 625 nm of a typical ZnP–C_{60} dyad in *o*-dichlorobenzene (*o*-DCB) and PhCN and Ref-ZnP in toluene at RT (λ_{ex} = 410 nm).[27]

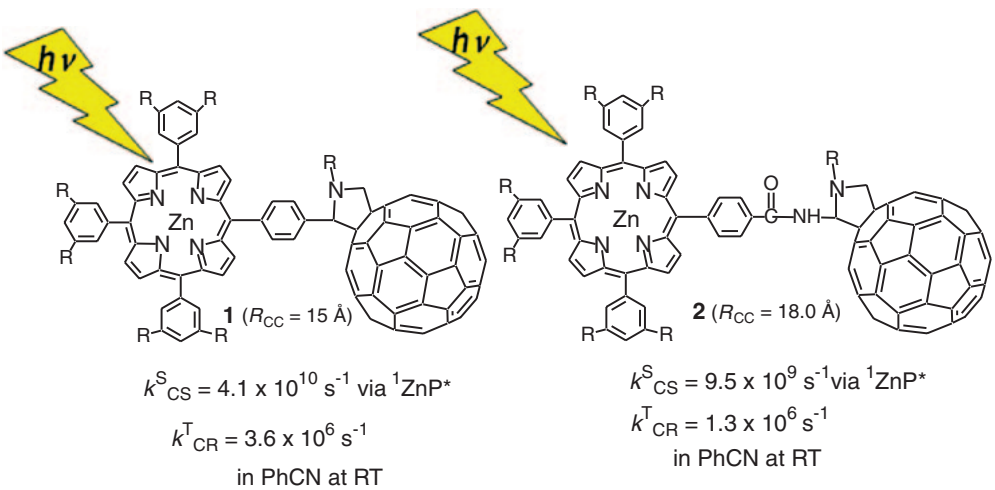

Figure 6. Rate constants of porphyrin–bridge–fullerene (ZnP–B–C_{60}) molecular systems (compound **1**[25] and compound **2**[26]).

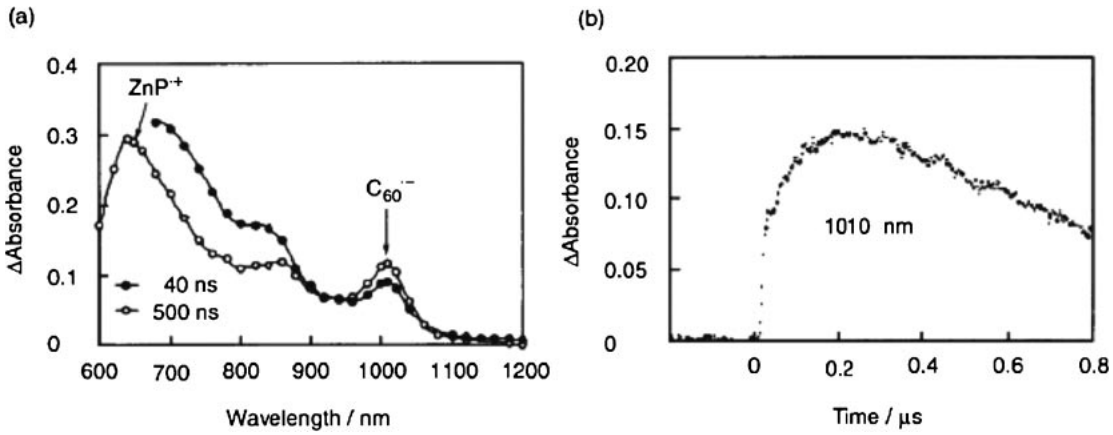

Figure 8. (a) Nanosecond transient absorption spectra of compound **2** and (b) time profile at 1000 nm in Ar-saturated PhCN at RT.[26]

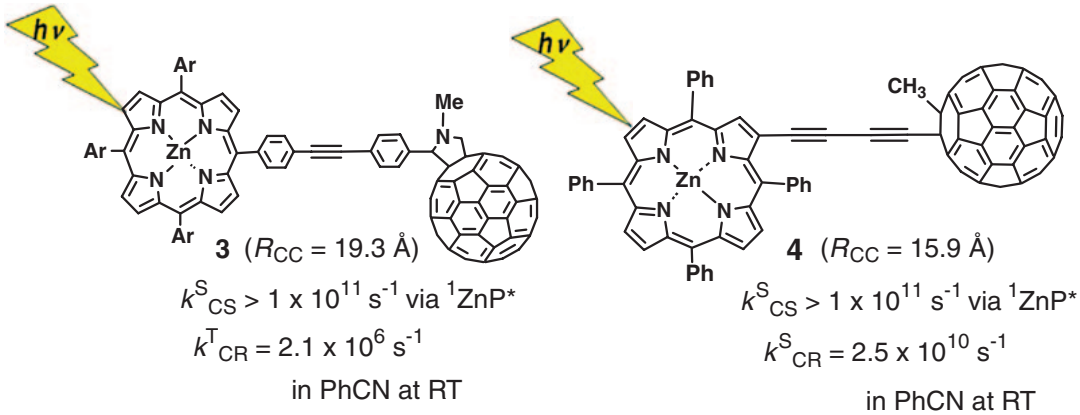

Figure 9. The rate constants of ZnP–phenyleneacetylene–C_{60} (compound **3**)[30] and ZnP–acetylene–C_{60} (compound **4**).[31]

is slowly regenerated. From the decay of the $C_{60}^{\bullet-}$-absorption band at 1000 nm, CR of the long-lived triplet state radical ion pair was determined to be $k^{T}_{CR} = 3.6 \times 10^{6}\,s^{-1}$ at RT, which corresponds to the lifetime (τ_{RIP}) of $ZnP^{\bullet+}$–B–$C_{60}^{\bullet-}$ to be 280 ns for **1**[25] and $k^{T}_{CR} = 1.3 \times 10^{6}\,s^{-1}$ and $\tau_{RIP} = 770$ ns for **2**.[26] In the CR process, the endothermic migration from the HOMO of B to the half-vacant HOMO of $ZnP^{\bullet+}$ or from the half-filled LUMO of $C_{60}^{\bullet-}$ to the LUMO of B (Figure 3) may be responsible to the observed slow CR.

On insertion of an acetylene bond between two phenyl rings as in compound **3** in Figure 9, Imahori et al. reported that CR is slightly faster than in shorter bridges; i.e., $k^{T}_{CR} = 2.1 \times 10^{6}\,s^{-1}$ and $\tau_{RIP} = 470$ ns at RT for compound **3**.[30] This observation may imply a rise of the HOMO energy level and lowering of the LUMO energy level of B compared with the corresponding MO levels of the amide bond of compound **2**. These changes in the LUMO of B decrease the energy barriers of the electron transfer from ZnP* to B in the CS (CS-1). In the CR, the magnitude of the rate constants may be determined by the energy barriers from the HOMO of B to the half-vacant HOMO of $ZnP^{\bullet+}$ or from the half-filled LUMO of $C_{60}^{\bullet-}$ to the LUMO of B. These changes result in faster CS and CR compared with compound **2** with a similar R_{CC} value.

In compound **4** with two acetylene bonds (Figure 9),[32] Vail et al. reported very fast electron transfer for both CS and CR compared with that of compound **3** with phenyl spacers at both ends of the acetylene bond. These observations indicate that the phenyl ring in compound **3** retards ET. This suggests that the electron jump from the HOMO of B to the half-vacant HOMO of $ZnP^{\bullet+}$ (CR-1) or from the half-filled LUMO of $C_{60}^{\bullet-}$ to the vacant LUMO of B (CR-1′) may be the rate determining processes in the CR of compound **3** (Figure 3).

On inserting the phenyl ring between ZnP and the bis-acetylene bridge as in compound **5** (Figure 10), Vail et al. reported that the rates of CS and CR were determined to be $k^{S}_{CS} = 2.3 \times 10^{10}\,s^{-1}$ and $k^{T}_{CR} = 3.1 \times 10^{6}\,s^{-1}$ ($\tau_{RIP} = 300$ ns) in PhCN at RT, which are slower than those of compound **4**, confirming that the phenyl ring acts as a resistive element for electron transfer through the bis-acetylene bridge.[32]

By further insertion of a phenyl group between the acetylene bond and C_{60} in compound **6** (Figure 10),[33] the ET rates slightly slow down compared with compound **5**. This implies that CR through the HOMO of the bis-acetylene bridges is more probable than that through the LUMO of the bis-acetylene bridges in Figure 3, because the phenyl group near the C_{60} retards the jump of electrons from the half-filled LUMO of the $C_{60}^{\bullet-}$ to the LUMO of the bis-acetylene bridges.

Extending the number of acetylene units from compound **5** to compounds **7** and **8**, the R_{CC} values increase from 18 to 23 Å (Figure 11). The k^{S}_{CS} values decrease only by ca. 1/3 with a

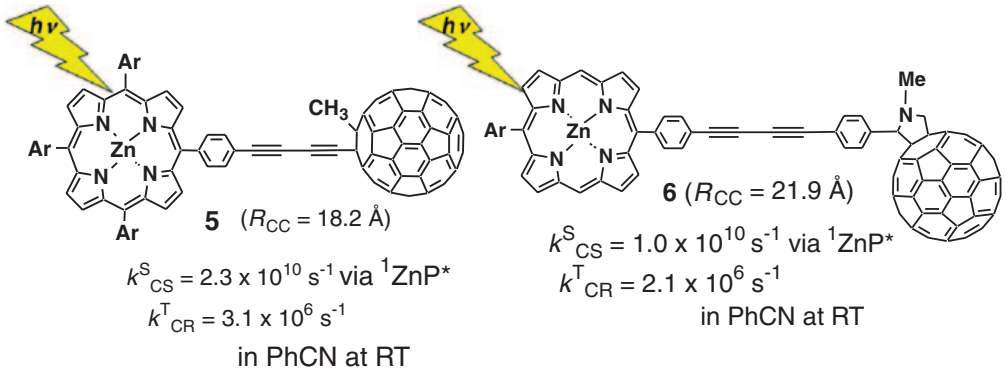

Figure 10. Rate constants of ZnP–phenyleneacetylene–C_{60} (compounds **5**[32] and **6**[33]).

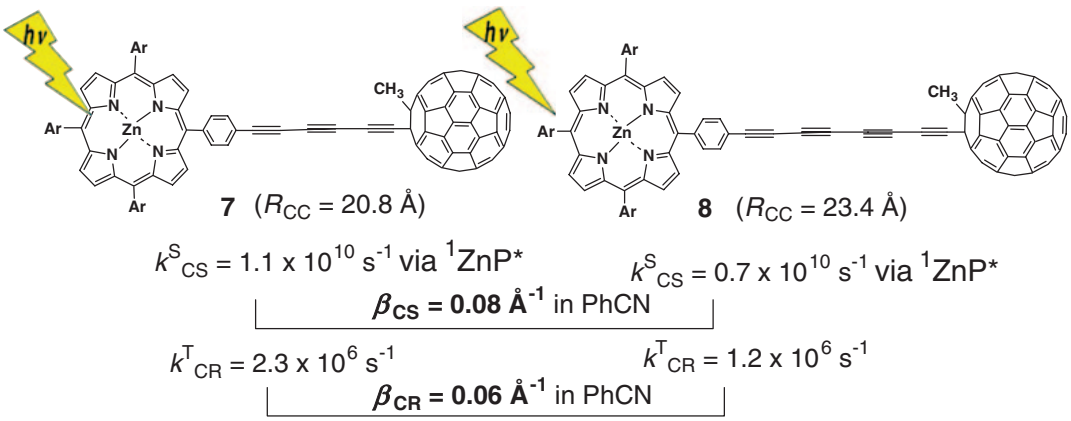

Figure 11. Rate constants of ZnP–oligoacetylene–C_{60} (compounds **7** and **8**).[32]

change of 5 Å, which gives a quite small damping factor (β_{CS}) of 0.08 $Å^{-1}$ in PhCN at RT.[32] This β_{CS} value is in good agreement with the reported value for bis-porphyrins connected by oligoacetylenes (0.08 $Å^{-1}$ in THF) reported by Osuka et al.[34] Such a small β_{CS} value evaluated from compounds **5**, **7**, and **8** suggests that CS takes place via ^{1}ZnP* even when the R_{CC} value is as great as 50 Å; however with larger R_{CC} values, the ISC of the ^{1}ZnP* state to the ^{3}ZnP* state ($k_{ISC} = 5 \times 10^8\ s^{-1}$) may become predominant over CS. The k_{CR} values also decrease with the R_{CC} values between the electron and the hole, giving $\beta_{CR} = 0.06\ Å^{-1}$ in PhCN at RT. The β_{CR} value is slightly smaller than the β_{CS} value, reflecting better electron-transferring ability through the HOMO than the LUMO of these bridges.

As shown in Figure 12, the energy levels of the LUMO of the oligoacetylenes become lower with increasing length, because the π-conjugation of the bridge spreads with the length.[35] Thus, the barrier for ET from the half-filled LUMO of ZnP to the LUMO of the oligoacetylene bridge (CS-1) becomes lower, resulting in large k_{CS} values for the longer bridges such as compounds **7** and **8**, as well as small β_{CS} values. With longer oligoacetylenes, the HOMO energy levels become higher, which results in lowering the jump energy from the HOMO of the bridges to the half-vacant HOMO of the $ZnP^{\bullet+}$ moiety (CR-1). Furthermore, decrease of β_{CR} is observed experimentally.[32] The electron conductivity along the LUMO of oligoacetylene must be different from that along the HOMO, because the number of nodes of the LUMO is usually greater

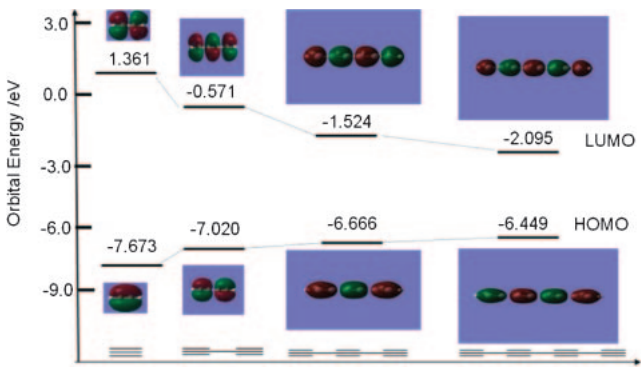

Figure 12. The HOMO and LUMO of the oligoacetylenes calculated by *Gaussian 03* DFT at B3LYP/6-31(d,p) level.[35]

than that of the HOMO. These β_{CR} values slightly smaller than the β_{CS} values for the oligoacetylene bridge (Figure 11) may reflect this difference.

The above observations are summarized as an energy diagram shown in Figure 13; the CS process must be electron transfer along the LUMO of the bridges, whereas the CR process must be electron transfer along the HOMO. A β_{CR} value slightly smaller than the β_{CS} value for the same oligoacetylene bridge (Figure 11) indicates a higher electron-transferring ability along the HOMO than that along the LUMO. In addition, the switching of electron-transfer mechanism from super-exchange to electron hopping occurs with

bridge length accompanied by the energy-level changes of the HOMO and LUMO of the bridges.

In the case of the phenyleneacetylene bridges as shown in Figure 14,[36] as the distances increase from 22 to 40 Å from compounds **6** to **10**, the k^{S}_{CS} values decrease drastically to about 1/100, which gives a quite large damping factor ($\beta_{CS} = 0.25$ Å^{-1} for the phenyleneacetylene bridges in PhCN at RT) as compared with the β_{CS} (=0.08 Å^{-1})[32,34] for the oligoacetylene bridges. The observed $\beta_{CS} = 0.25$ Å^{-1} suggests that CS via ^{1}ZnP* is competitive with the ISC to ^{3}ZnP* in R_{CC} longer than ca. 35 Å. This relatively large β_{CS} value suggests that the phenyl group in the middle of the acetylene bonds acts as a resistor for electron conduction along the LUMO of the phenyleneacetylene bridges.

Competition between ISC and CS via ^{1}ZnP*, which is expected to be dependant on the length of the phenyleneacetylene bridges, can be confirmed by nanosecond transient spectra as shown in Figure 15. In the shortest bridge (compound **1**), the sharp absorption of $C_{60}^{\bullet-}$ can be observed at 1000 nm. Furthermore, the absorption at 680 nm of $ZnP^{\bullet+}$ is also sharp. This spectrum indicates that CS predominantly takes place, because of k^{S}_{CS} (=4.1 × 10^{9} s^{-1}) ≫ k_{ISC} (=5 × 10^{8} s^{-1}). For compound **6**, similar sharp absorption peaks were observed at 1000 and 680 nm, in addition a new peak appears at 740 nm, which can be attributed to $^{3}C_{60}$*, suggesting increase of ISC. With further increase in the length of the phenyleneacetylene bridges (compounds **6** and **9**), the absorption band at 1000 nm becomes broader, while the absorption bands due to ^{3}ZnP* increase at 800 and 750 nm, in addition to the absorption of $^{3}C_{60}$*, since the k^{S}_{CS} values approach the same order of the ISC rate constant. Usually, the k_{CR} values can be evaluated from the decay of the $C_{60}^{\bullet-}$ absorption at 1000 nm, because the absorption of $ZnP^{\bullet+}$ in the 620–680 nm region overlaps with the absorptions of the triplet states. Thus, the k_{CR} values for compounds **1** and **6** are quite reliable, whereas the decays at 1000 nm for compounds **9** and **10** are complicated due to the overlap with other species. In particular, the slow decay regions at longer times may be a superposition of the decay of ^{3}ZnP* and $^{3}C_{60}$*. Thus, these k_{CR} values in Figure 14 must be used carefully taking these situations into consideration.

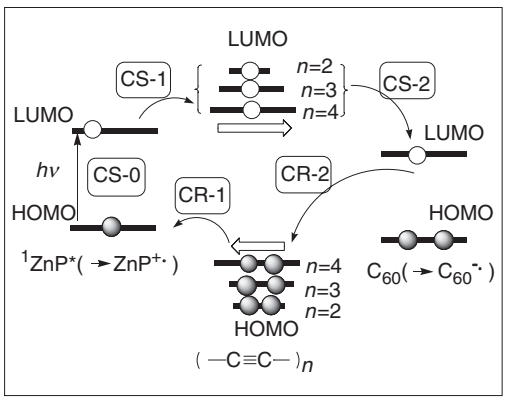

Figure 13. Schematic illustration of the energy diagram of compounds **5**, **7**, and **8**.

The MOs of compound **6** are shown in Figure 16 as an example, in which the HOMO is localized on the ZnP moiety, while the LUMO is localized on the C_{60} moiety, suggesting that the most stable CS state is $ZnP^{\bullet+}$–phenyleneacetylene–$C_{60}^{\bullet-}$. Although HOMO−1 is also localized on the ZnP moiety similar to the HOMO, HOMO−2 is localized on the phenyleneacetylene bridge and its energy level is slightly lower than those of the HOMO and HOMO−1 of compound **6**. Although the LUMO+n (n = 1–4) are localized on the C_{60} group similar to the LUMO, the LUMO+5 is localized on the ZnP, which corresponds to the locally excited state of the ZnP. From the half-filled LUMO+5, the electron jumps up to the LUMO+14 localized on the phenyleneacetylene bridge, through which the electron transfers to the LUMO localized on C_{60} in CS. In the CR, an electron of the HOMO−2 localized on the phenyl-

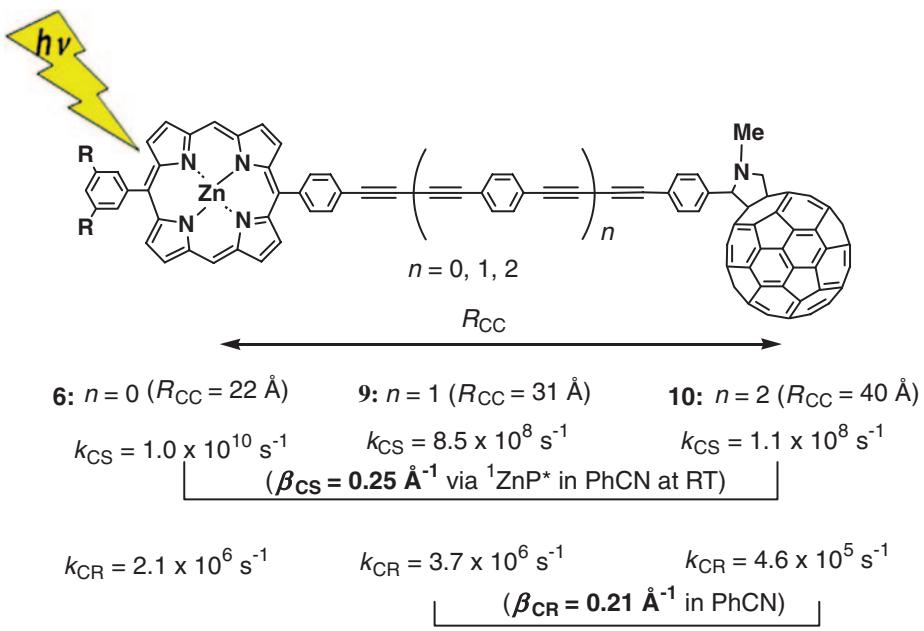

Figure 14. Rate constants of ZnP–phenyleneacetylene–C_{60} (compounds **6**, **9**, and **10**).[36]

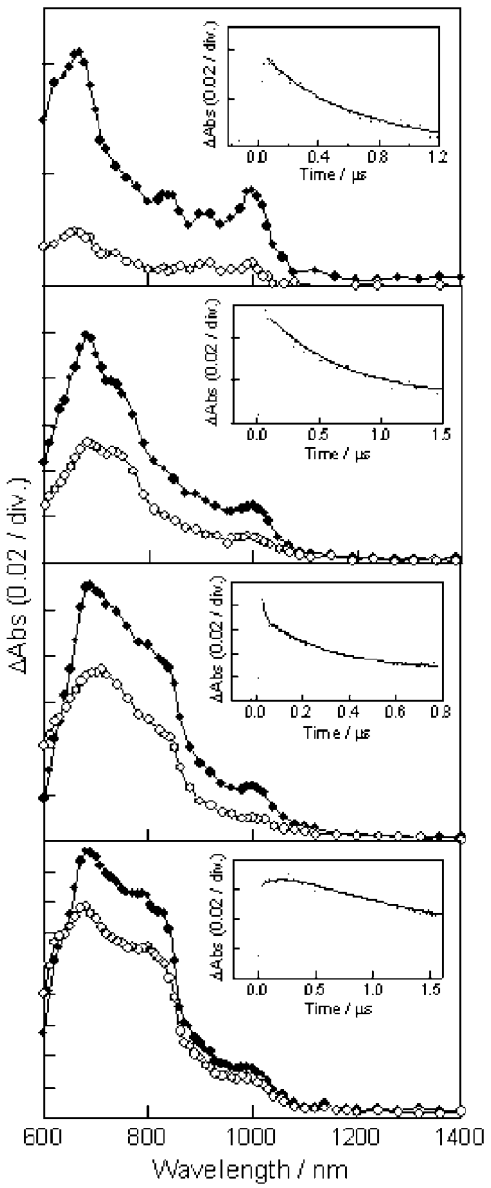

Figure 15. Nanosecond transient absorption spectra at 0.1 (●) and 1.0 μs (○) of compounds **1**, **6**, **9**, and **10** from up to down; (inset) time profile at 1000 nm in Ar-saturated PhCN at RT.[25,33]

eneacetylene bridge jumps up to the half-vacant HOMO localized on the $ZnP^{\bullet+}$, then an electron of the half-filled LUMO localized on $C_{60}{}^{\bullet-}$ falls to compensate the half-vacant HOMO−2.

Comparing the MOs along the di-acetylene unit of compound **6** in Figure 16,[25,35] the numbers of nodes of the HOMO and LUMO of di-acetylene are 2 and 3, respectively, which are similar to those of the di-acetylene in Figure 12. However, in the phenyl rings on both sides there are nodes which may inhibit the delocalization of the electron, acting as a resistive element for electron and hole conductions. Similar MOs were evaluated for compounds **9** and **10**.

The energy levels of the LUMO+*n* localized on the oligophenyleneacetylene bridges of compounds **6**, **9**, and **10** are almost the same within ca. 0.3 eV as shown in Figure 17.

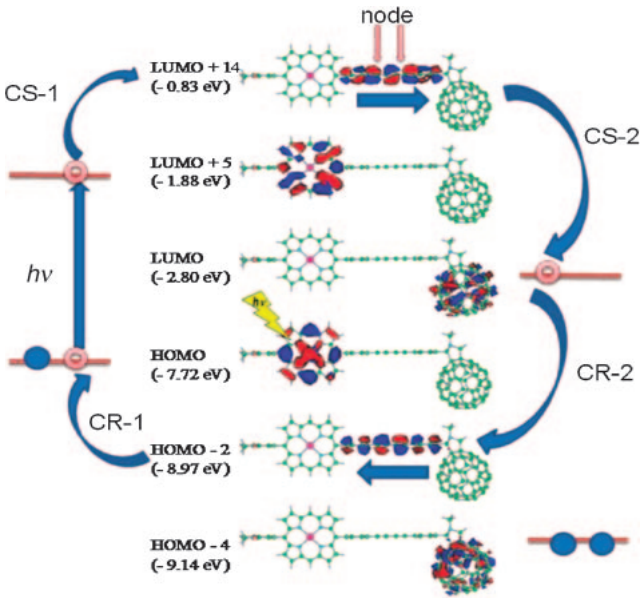

Figure 16. The scheme of photoinduced electron transfer based on the molecular orbitals of compound **6** calculated by *Gaussian 03* at PM3 level.[25,35]

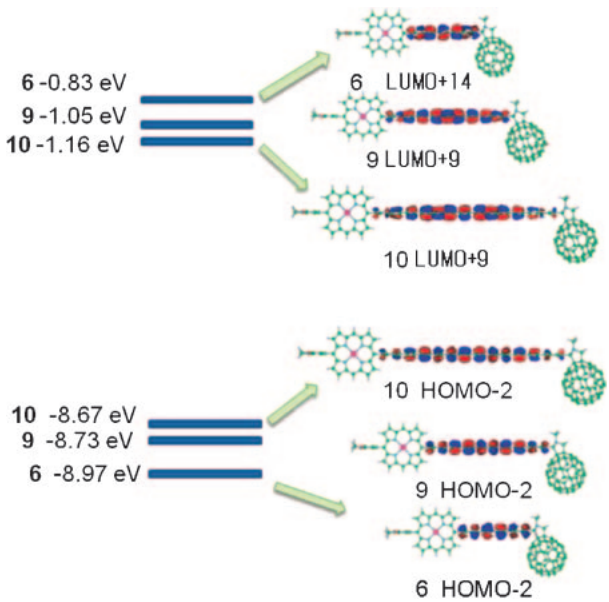

Figure 17. The molecular orbitals localized on the oligophenyleneacetylene bridges between the ZnP and C_{60} moieties of compound **6**, **9**, and **10** calculated by *Gaussian 03* at PM3 level.[25]

The energy levels of HOMO−2 localized on the oligophenyleneacetylenes of compounds **6**, **9**, and **10** are also quite similar within ca. 0.3 eV. These energy differences of the phenyleneacetylene bridges are quite small compared with the energy difference of the oligoacetylenes for compounds **5**, **7**, and **8** in Figure 12. Thus, the electron-transferring abilities along the oligophenyleneacetylene bridges apart from the LUMO of the ZnP and the HOMO of the $ZnP^{\bullet+}$ depend only on the distance, giving a large β_{CS} (0.25 $Å^{-1}$ in PhCN at RT), which is predominantly due to super-exchange. This β_{CS} value is 3 times larger than that through the oligoacetylene bridges, in

which the energy levels approach those of ZnP and C_{60} with length, resulting in an increase in contribution of the hopping mechanism, which can compensate for the electron-transfer damping due to the distance.

On the other hand, phthalocyanine (ZnPc) and C_{60} dyads with acetylene bridges have been recently reported by Quintiliani et al.[37] Quite fast intramolecular CS and CR processes were evaluated. The rate constants for CS and CR of ZnPc–acetylene–C_{60}, in which the acetylene moiety is directly connected to both ZnPc and C_{60}, are almost the same as those of the indirect connection cases (i.e., insertions of an ethane linkage), suggesting that CS and CR take place via the super-exchange mechanism. Quite large solvent polarity changes have been reported for the rates of CS and CR of ZnPc–acetylene–C_{60}; i.e., the k_{CR} values are $(2–3) \times 10^{10}\,s^{-1}$ in PhCN at RT, whereas they are ca. $1 \times 10^{8}\,s^{-1}$ in toluene at RT.[37] This trend is consistent with Marcus theory, predicting that instability of $ZnPc^{\bullet+}$–acetylene–$C_{60}^{\bullet-}$ in toluene brings the CR to deeper inverted region corresponding to the small reorganization energy due to spherical $C_{60}^{\bullet-}$.[22] In the case of the ZnP–bridge–C_{60}, however, such a large solvent polarity change was not observed.

It is interesting to compare these oligophenyleneacetylene bridges with the phenylenevinylene bridges. ZnP–oligophenylenevinylene–C_{60} molecular systems (compounds **11** and **12** in Figure 18) have been reported by de la Torre et al.[38] The CS process via ^{1}ZnP* was confirmed by pico-seconds transient absorption spectra and the k^S_{CS} values were calculated to be $(3.2–4.5) \times 10^{9}\,s^{-1}$ for compounds **11** and **12**. As for the CR, the k_{CR} values were reported in the range of $(0.9–4.4) \times 10^{6}\,s^{-1}$ in PhCN and THF at RT. These k^S_{CS} and k_{CR} values are similar to those of other ZnP–B–C_{60} molecular systems including ZnP–oligophenyleneacetylene–C_{60}. From the MO considerations, it is presumed that the energy difference between the half-filled LUMO localized on $C_{60}^{\bullet-}$ and the LUMO of the oligophenylenevinylene bridges is larger than that between the HOMO of the oligophenylenevinylene bridges and the half-vacant HOMO of the $ZnP^{\bullet+}$ moiety, suggesting that CR takes place via CR-1 rather than CR-1′ in Figure 3.

From these k^S_{CS} and k_{CR} values for compounds **11** and **12** and other related compounds, the β_{CS} and β_{CR} values were determined to be less than $0.04\,Å^{-1}$ in PhCN at RT,[38] which are almost the same as the reported β_{CS} values for other molecular systems with oligophenylenevinylene bridges ($\beta_{CS} = 0.04\,Å^{-1}$).[7,38] These β_{CS} values are far smaller than the β_{CS} of the oligophenyleneacetylene bridges ($0.25\,Å^{-1}$).[36] The $\beta_{CS} = 0.03\,Å^{-1}$ implies that CS via ^{1}ZnP* is possible even when R_{CC} is ca. 100 Å, until ISC of ^{1}ZnP* is competitive. The energy difference of the HOMO$-m$ between tetraphenylenevinylene and hexaphenylenevinylene is ca. 0.1 eV and that of the LUMO$+n$ is also 0.1 eV. These small energy differences suggest that the observed small β_{CS} and β_{CR} values must be attributed to the high electron-transferring ability of the oligophenylenevinylenes. Since larger β_{CS} values were reported for oligovinylene bridges ($\beta_{CS} = 0.1\,Å^{-1}$ in THF at RT) by Sikes et al.,[39] it can be pointed out that the phenyl moieties among the vinylene units do not retard electron transfer through the LUMO and HOMO; rather the phenyl groups between the vinylene units seem to promote remote

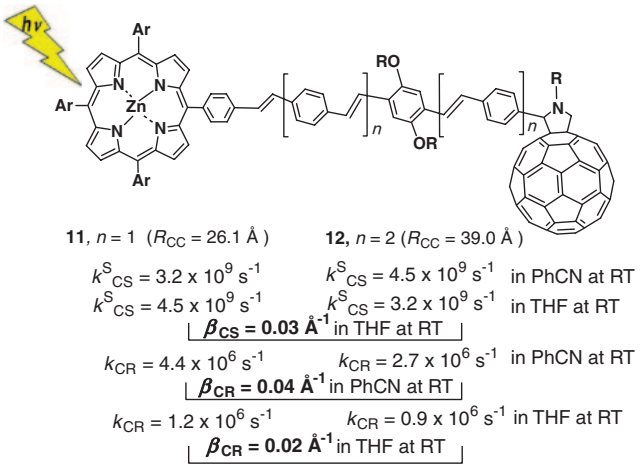

Figure 18. Rate constants of ZnP–oligophenylenevinylene–C_{60} (compounds **11** and **12**).[38]

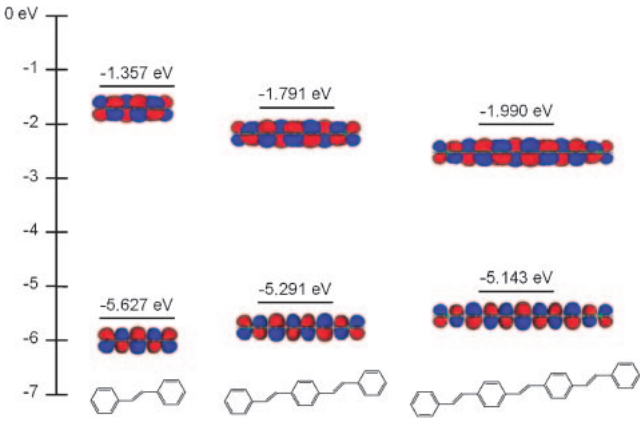

Figure 19. The HOMO and LUMO of oligophenylenevinylenes calculated by *Gaussian 03* DFT at B3LYP/3-21 level.[35]

electron migration.

The LUMO and HOMO of the oligophenylenevinylenes are shown in Figure 19, which reveals that the LUMOs delocalize over the entire phenylenevinylene. The energy levels of the LUMOs considerably decrease with the number of phenylenevinylene units. The difference of the energy levels between mono- and diphenylenevinylene is 0.4 eV, whereas it becomes as small as 0.2 eV between di- and triphenylenevinylene. These values are larger than those of the phenyleneacetylene bridges (Figure 12). Thus, it is suggested that inter-conversion of the electron-transfer mechanism is possible from super-exchange to electron-hopping with the length of the phenylenevinylene bridges. As for the shape of the MO clouds, the overlapping with vicinal clouds of the LUMO seems to be more prominent compared with that of the HOMO, although there are more nodes present than in the HOMO.

Since almost the same energy changes for the HOMO and the LUMO were obtained for phenylene–bisvinylene units,[35] which are analogs of the phenylene–bisacetylene units in Figure 12, the relatively large energy differences obtained here are characteristic of the phenylenevinylenes.

The MOs of the vinylenes are also shown in Figure 20 as comparison. Surprisingly enough, the number of nodes in the

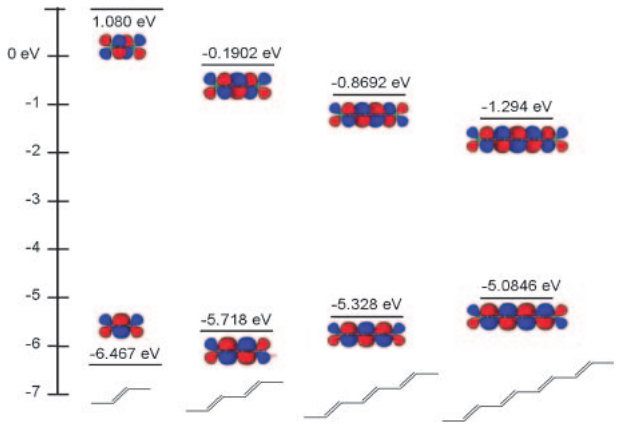

Figure 20. The HOMO and LUMO of oligovinylenes calculated by *Gaussian 03* DFT at B3LYP/3-21 level.[35]

LUMO is more than that of the phenylenevinylene, suggesting that the phenyl group between the vinylenes acts as a mediator for the delocalization of the π-clouds even in the LUMO. Thus, it would be anticipated that the phenyl group between the vinylenes acts as accelerator for electron transfer, which reasonably explains the observed low β_{CS} values in Figure 18. This is a strong contrast with the LUMO of the phenylene–diacetylene bridges, in which clear nodes exist on the phenyl ring of the LUMO (Figure 12).

When the oligothiophenes (*n*T) are employed as bridges for CS from the photo-excited porphyrin (MP*) to the C_{60} (Figure 21),[40,41] the electron-transfer mechanism appears to change with the length of *n*T units, since the HOMO–LUMO gaps of the *n*T units decrease approaching the HOMO–LUMO gap of the porphyrin and C_{60} moieties.

The optimized structures of MP–*n*T–C_{60} calculated assuming a polar solvent show the π-delocalization in whole *n*T units, although the *n*T units slightly twist along the chains.[40,41] From H_2P–4T–C_{60} (compound **13**) to H_2P–12T–C_{60} (compound **15**), the R_{CC} values vary as much as 30 Å from 26 to 56 Å. The observed absorption spectrum of MP–*n*T–C_{60} is almost overlapped with the summed spectrum of the components, suggesting almost no appreciable interaction among the components in the ground state. This is supported by the optimized structure in which the porphyrin ring is almost perpendicular to the vicinal thiophene ring, cutting the π-conjugation between them. Although the absorption of the 12T unit appearing at 480 nm is longer than that of 4T (380 nm), it is still shorter than the Q-band of the H_2P moiety (550–600 nm) and the longest absorption of the C_{60} at 700 nm. Thus, the HOMO–LUMO gap of the *n*T units is slightly wider than the those of H_2P and C_{60}, suggesting that the super-exchange mechanism is still predominantly working. However, with increasing length of *n*T units, the oxidation potentials of the *n*T units decrease approaching that of H_2P, suggesting that the electron-hopping mechanism is possible.

Steady-state fluorescence spectra of MP–*n*T–C_{60} observed by exciting the MP with 420-nm light show a fluorescence band at 600–700 nm due to the MP. Since the fluorescence intensity of a MP–*n*T molecule is almost the same as that of a MP molecule, no appreciable interaction is present between the ^{1}MP* and the *n*T units. On the other hand, by further

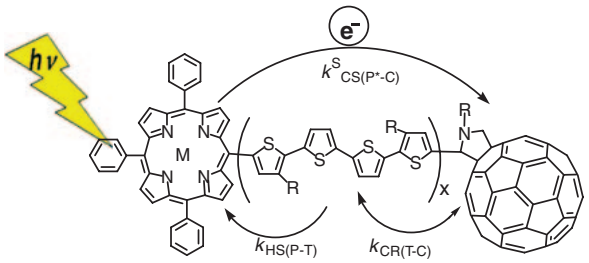

13: H_2P-4T-C_{60} (R_{CC} = 26 Å) | **14**: H_2P-8T-C_{60} (R_{CC} = 40 Å) | **15**: H_2P-12T-C_{60} (R_{CC} = 56 Å)

$k^S_{CS(^1H_2P^*-C)}$ = 1.7 x 10^9 s^{-1} | 1.6 x 10^9 s^{-1} | 0.7 x 10^9 s^{-1}

β_{CS} = 0.03 $Å^{-1}$ in PhCN at RT

$k_{HS(P-T)}$ = 3.5 x 10^8 s^{-1} | 7.7 x 10^7 s^{-1} | 7.0 x 10^7 s^{-1}

$k_{CR(T-C)}$ = 4.2 x 10^5 s^{-1} | 5.2 x 10^5 s^{-1} | 6.9 x 10^5 s^{-1}

in PhCN at RT

16: ZnP-4T-C_{60} (R_{CC} = 26 Å) | **17**: ZnP-8T-C_{60} (R_{CC} = 40 Å)

$k^S_{CS(^1ZnP^*-C)}$ = 5.0 x 10^9 s^{-1} | 6.8 x 10^8 s^{-1}

β_{CS} = 0.14 $Å^{-1}$ in PhCN at RT

$k_{HS(P-T)}$ = 6.6 x10^8 s^{-1} | 1.6 x 10^8 s^{-1} in *o*-DCB at RT

$k_{CR(T-C)}$ = 1.6 x10^6 s^{-1} | 1.2 x 10^6 s^{-1} in PhCN at RT

Figure 21. Rate constants of MP–*n*T–C_{60} (M = H_2, compounds **13**, **14**, and **15** and M = Zn compounds **16** and **17**).[40,41]

connection of the C_{60} at the end of *n*T, the fluorescence intensity of the MP decreases to ca. 1/10. In non-polar toluene, an additional fluorescence peak appears at 720 nm due to C_{60}, indicating the EnT from ^{1}MP* to C_{60}, whereas C_{60}-fluorescence was not observed in PhCN, indicating predominant CS from ^{1}MP* to C_{60}. Even by the selective excitation of the *n*T units of MP–*n*T–C_{60}, no steady-state fluorescence due to the *n*T was observed, because of the rapid relaxation within the *n*T units and with interaction with the vicinal C_{60}.[42]

These steady-state fluorescence-quenching phenomena are all tracked by time-resolved fluorescence measurements as follows. Although the time profiles of MP-fluorescence of MP–*n*T dyads are almost the same as pristine MP-fluorescence, drastic shortening of the MP-fluorescence was observed for MP–*n*T–C_{60}. In PhCN, CS from the ^{1}MP* to the C_{60} mainly takes place through the *n*T units. In toluene on the other hand, EnT takes place from ^{1}MP* to the C_{60} through the *n*T units.[40,41]

In polar solvents, evidence for radical ion pair generation from initial CS via ^{1}MP* was obtained by pico-second transient absorption spectra. After a 150 femto-second laser pulse, the transient absorption of ^{1}MP* was observed in the 500–600 nm region. After the decay of ^{1}MP*, the absorption bands of $MP^{\bullet+}$ and $C_{60}^{\bullet-}$ appear and remain for 10–100 ps, supporting the initial generation of $MP^{\bullet+}$–*n*T–$C_{60}^{\bullet-}$. The CS rate constants via ^{1}MP* are referred to as $k^S_{CS(P^*-C)}$ in Figure 21. Afterward, $MP^{\bullet+}$–*n*T–$C_{60}^{\bullet-}$ is converted to MP–$nT^{\bullet+}$–$C_{60}^{\bullet-}$ by hole-shift ($k_{HS(P-T)}$), since the absorption of $nT^{\bullet+}$ was observed in the nanosecond transient absorption spectra. An example is shown in Figure 22 for ZnP–$8T^{\bullet+}$–$C_{60}^{\bullet-}$ (compounds **17**) in PhCN at RT.[41] The details of the electron- and hole-transfer mechanisms change with solvent

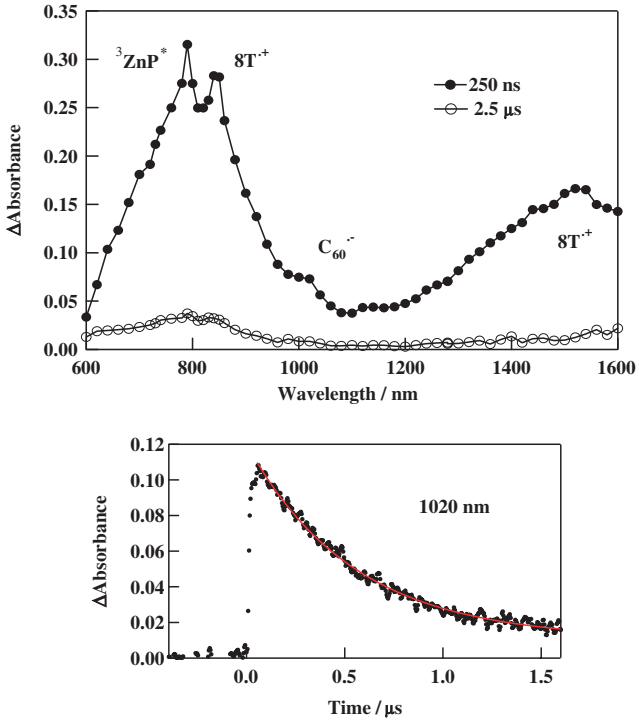

Figure 22. Nanosecond transient absorption spectra of ZnP–8T–C_{60} (compound **17**) in PhCN at 250 ns (●) and 2.5 μs (○) after 560-nm laser irradiation and absorption-time profiles at 1020 nm (lower panel).[41]

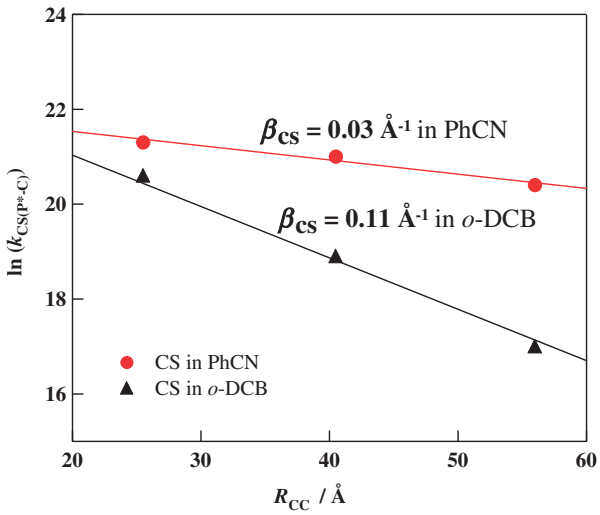

Figure 23. Dependence of the k^S_{CS} values for H_2P–*n*T–C_{60} via $^1H_2P^*$ on the R_{CC}.[40]

polarity.[41] At longer times, the rates of CR ($k_{CR(T-C)}$) were observed from the decay of MP–*n*T$^{\bullet+}$–$C_{60}^{\bullet-}$.

The $k^S_{CS(P^*-C)}$ values for H_2P–*n*T–C_{60} decrease with an increase in the R_{CC} values as shown in Figure 23. The β_{CS} value was evaluated to be 0.03 Å^{-1} in PhCN, which is as small as that of ZnP–oligophenylenevinylene–C_{60} (β_{CS} = 0.03 Å^{-1} in THF at RT),[38] indicating high electron-transferring ability of the *n*T units working as molecular wires. This small β_{CS} value implies that CS via $^1H_2P^*$ takes place even when the R_{CC} value reaches ca. 100 Å until ISC of $^1H_2P^*$ ($k_{ISC} = 1 \times 10^8$ s^{-1}) is

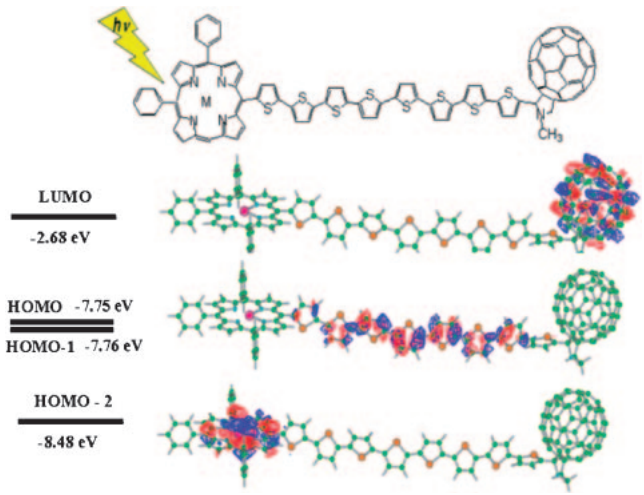

Figure 24. The MOs for ZnP–8T–C_{60} (compound **17**).[43]

competitive with CR via $^1H_2P^*$. In less polar *o*-DCB, the β_{CS} value increases up to 0.11 Å^{-1}, indicating that the polarity of the solvent considerably affects the β_{CS} value. This suggests that highly polar solvents stabilize the transferring electron on the LUMO of the *n*T units. Thus, it can be presumed that the electron residence time on the LUMO of these *n*T units is sufficiently long to be able to feel the solvent polarity; that is, the CS process takes place almost via the electron-hopping mechanism.

The MOs of ZnP–8T–C_{60} (compound **17**) are shown in Figure 24, from which it is revealed that the HOMO and HOMO−1 are localized on the 8T unit and the HOMO−2 is localized on the ZnP, whereas the LUMO is localized on the C_{60}.[43] Therefore, both ZnP–8T$^{\bullet+}$–$C_{60}^{\bullet-}$ and ZnP$^{\bullet+}$–8T–$C_{60}^{\bullet-}$ are expected to be stable charge-separated radical ion pairs.[39] The next higher LUMO is localized on the ZnP moiety, which corresponds to the first excited state of ZnP, from which the electron transfers to the LUMO localized on C_{60} through the higher LUMO localizing on the 8T unit. The most important factor leading to the small β_{CS} value is the electron-transferring ability of the *n*T units through the higher LUMO, in which π-electron delocalizes in whole *n*T units.

Combining the observed oxidation and reduction potentials with the MO calculation data, the energy diagrams for CS and CR of H_2P–*n*T–C_{60} can be schematically illustrated as shown in Figure 25. Compared with the oligoacetylene bridges shown in Figure 11, in which the electron hopping through the oligoacetylene bridges is imaginary, the HOMO levels of the *n*T units are as high as the HOMO of the MP moiety. Thus, in CR of ZnP$^{\bullet+}$–*n*T–$C_{60}^{\bullet-}$, the electron-shift from *n*T to MP is possible generating ZnP–*n*T$^{\bullet+}$–$C_{60}^{\bullet-}$, when *n*T becomes long. That is, electron hopping through the *n*T units is real as seen in Figure 22. In the CS process, the absorption of *n*T$^{\bullet-}$ was not observed even in the picoseconds time region, which implies that the electron hopping through the LUMO of *n*T is still imaginary, although the contribution of the hopping mechanism may increase with the length of *n*T.

It is notable that CR between vicinal radical ion pair ZnP–*n*T$^{\bullet+}$–$C_{60}^{\bullet-}$ is as slow as 10^5–10^6 s^{-1}, which are similar rates to those of the slow CR for *n*T$^{\bullet+}$–$C_{60}^{\bullet-}$.[44,45] Such a slow process

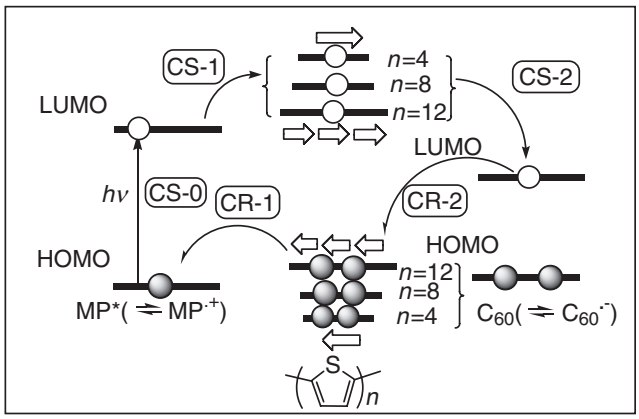

Figure 25. Schematic illustration of photo-induced electron transfer via MP*, in which the contribution of electron hopping to CR increases with increase in the *n*T units.

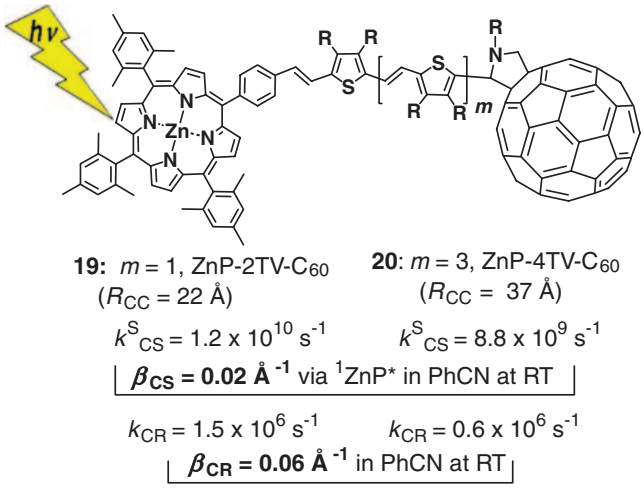

Figure 27. Rate constants of ZnP–*n*TV–C_{60} (compound **19**, $n = 2$ and compound **20**, $n = 4$).[48]

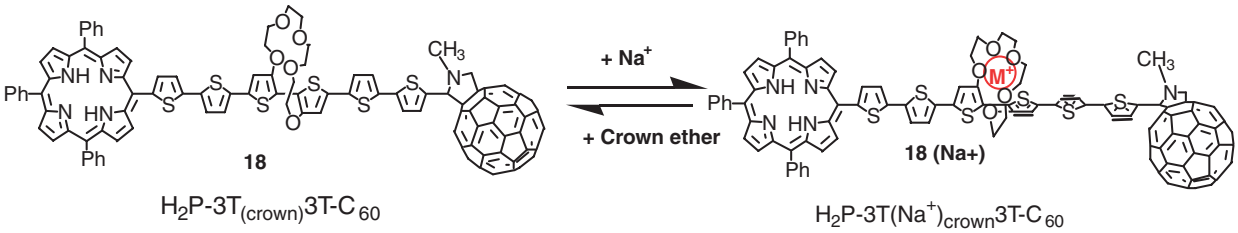

Figure 26. Switching the CS with Na^+ for H_2P–$3T_{(crown)}3T$–C_{60} (compound **18**).[46]

between nT$^{\bullet+}$–$C_{60}^{\bullet-}$ is rationalized by taking the Marcus inverted region and triplet spin state into consideration.[44,45]

In order to control ET along the *n*T units, crown ether is inserted in the center of the 6T unit as shown in Figure 26 (H_2P–$3T_{(crown)}3T$–C_{60}: compound **18**).[46] Without Na^+, the 6T unit connecting H_2P and C_{60} is planar, delocalizing the π-electrons over the entire 6T moiety. Therefore, rapid CS takes place via $^1H_2P^*$ as proven by the accelerated $^1H_2P^*$-fluorescence quenching by C_{60}; indeed, the prolonged radical ion pair H_2P–$(3T_{(crown)}3T)^{\bullet+}$–$C_{60}^{\bullet-}$, which is generated from the initially produced $H_2P^{\bullet+}$–$3T_{(crown)}3T$–$C_{60}^{\bullet-}$ via hole-shift, was confirmed by the transient absorption bands of $6T^{\bullet+}$ and $C_{60}^{\bullet-}$.[46] On addition of excess Na^+, H_2P–$3T(Na^+)_{crown}3T$–C_{60} (=compound **18**(Na^+)) is formed in PhCN, which decelerates the $^1H_2P^*$-fluorescence decay, approaching the rate of pristine $^1H_2P^*$, suggesting that CS from $^1H_2P^*$ to C_{60} is prohibited. Indeed, only the triplet states of the components were observed in the transient absorption spectra instead of the radical ions. These observations suggest that the π-conjugation of 6T is cut by Na^+ insertion in the crown ether and disruption of the planarity of 6T.[47] By further addition of the 15-crown ether-5 extracting Na^+ from H_2P–$3T(Na^+)_{crown}3T$–C_{60}, the rapid decay of the $^1H_2P^*$-fluorescence was recovered and the transient absorption bands of the radical ions reappeared, indicating the re-generation of flat 6T for H_2P–$3T_{(crown)}3T$–C_{60}, which leads to photoinduced CS again.[46]

As for the oligothiophenevinylene (*n*TV) bridges, the synthesis and photophysics of ZnP–*n*TV–C_{60} (compound **19** for $n = 2$ and compound **20** for $n = 4$) have been studied; some data are summarized in Figure 27.[48] The k^S_{CS} values evaluated from the ^{1}ZnP*-fluorescence are as large as ca. 1×10^{10} s^{-1}, which is larger than those of ZnP–*n*T–C_{60} and ZnP–oligophenylenevinylene–C_{60}. The β_{CS} value was found to be 0.02 Å^{-1} in PhCN at RT, although only two data are shown in Figure 27.[49] Such a small β_{CS} value implies that CS via ^{1}ZnP* takes place up to R_{CC} values of ca. 120 Å at which point ISC of ^{1}ZnP* is competitive. On the other hand, the k^S_{CR} values for ZnP$^{\bullet+}$–*n*TV–$C_{60}^{\bullet-}$ via ZnP–*n*TV$^{\bullet+}$–$C_{60}^{\bullet-}$, which were evaluated from the transient absorption spectra on a nanosecond time scale,[50] are as slow as ca. 1×10^6 s^{-1} in PhCN at RT. The presence of ZnP–*n*TV$^{\bullet+}$–$C_{60}^{\bullet-}$ on a nanosecond time scale indicates the ability of *n*TV as a hole trap similar to *n*T.

When Si–Si bonds are inserted between the acetylene bonds as a bridge as shown for compound **21** in Figure 28, many conformations may exist by rotation around the single bonds of –C≡C–Si–Si–C≡C– bridges.[51] Among many conformations, an extended structure and a folded structure are shown in Figure 29 as typical conformations.[52] Thus, the observed k^S_{CS} value of compound **21** is almost the same as those of compounds **5**, **6**, and **7**, which are the extended structures with similar R_{CC}. However, in the folded structure, EnT from ^{1}ZnP* to C_{60} may be competitive with CS even in polar solvent. For the generated radical ion pair, ZnP$^{\bullet+}$–C≡C–Si–Si–C≡C–$C_{60}^{\bullet-}$ was confirmed from nano-second transient absorption spectra; this type of radical ion pair can be also estimated from the HOMO localizing on ZnP and the LUMO localizing on the C_{60} in Figure 29.

The k_{CR} value for ZnP$^{\bullet+}$–C≡C–Si–Si–C≡C–$C_{60}^{\bullet-}$ is as small as the order of 10^6 s^{-1}, which also supports the existence

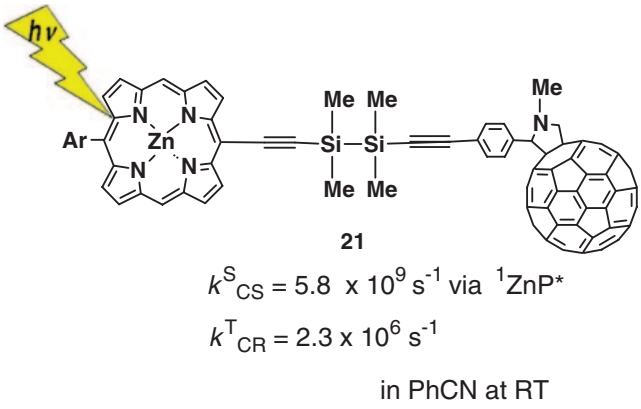

Figure 28. Rate constants of ZnP–bridge–C_{60} with the –C≡C–Si–Si–C≡C (compound **21**).[51]

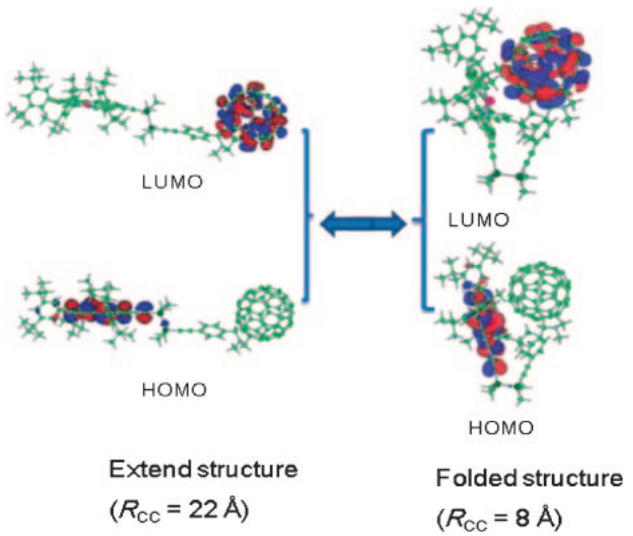

Figure 29. Two typical conformations of compound **21**, and their HOMO and LUMO.[52]

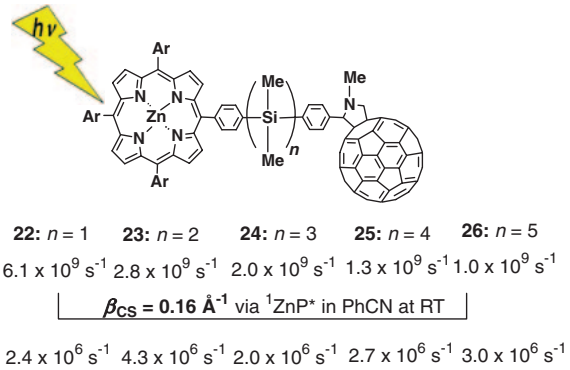

Figure 30. Rate constants of ZnP–$(Si)_n$–C_{60} (compounds **22**, **23**, **24**, **25**, and **26** for n = 1–5, respectively).[53]

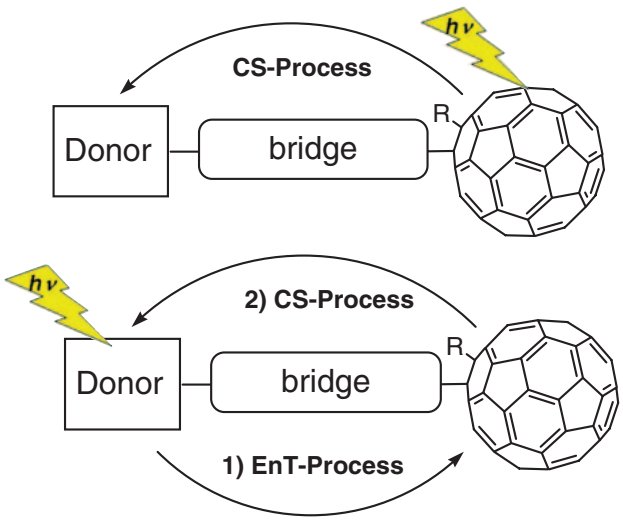

Figure 31. Fullerene excitation of donor–bridge–C_{60}; (upper panel) direct excitation and (lower panel) indirect excitation (after donor excitation, the EnT process takes place to C_{60}, from which CS takes place).

of the extended structure.

On inserting the –$(Si)_n$– bonds between two phenyl rings connected to the ZnP and C_{60} moieties, ZnP–$(Si)_n$–C_{60} (compounds **22**, **23**, **24**, **25**, and **26** for n = 1–5, respectively) were synthesized as shown in Figure 30.[53] They also exist as mixtures of various conformations in solution. The observed k^{S}_{CS} values via ^{1}ZnP* are in almost the same range as those of compounds **5**, **6**, and **7**, suggesting the existence of extended structures. These k^{S}_{CS} values for ZnP–$(Si)_n$–C_{60} decrease with the number of –$(Si)_n$– units, reflecting the ET through the Si–Si bonds. The β_{CS} value for ZnP–$(Si)_n$–C_{60} was determined to be 0.16 Å^{-1}, which is as small as the π-conjugated bridges; that is, between $\beta_{CS} = 0.08$ Å^{-1} for the oligoacetylene bridges[32] and $\beta_{CS} = 0.25$ Å^{-1} for the oligophenyleneacetylene bridges in PhCN at RT.[36] This β_{CS} value suggests that the Si–Si bonds have high electron-transferring ability along the LUMO of σ-bonds of the Si–Si units. On the other hand, the observed k^{T}_{CR} values are almost constant within (2.0–4.3) × 10^{6} s^{-1} as listed in Figure 30, which can be explained by two interpretations: One possible interpretation is that the rate-determining step of CR is the rates of the conformational change from the extended conformation to the folded conformation of ZnP$^{\bullet+}$–$(Si)_n$–$C_{60}^{\bullet-}$, in which CR takes place immediately. Another possible interpretation is the high hole-migration along the HOMO of the S–Si σ-bond in CR, independent of the –$(Si)_n$– length.

Fullerene Excitation for Donor–Bridge–C_{60} Molecular Systems

By the fullerene excitation of D–B–C_{60} systems, the CS process takes place via the HOMO of the bridge molecule as illustrated in Figure 4, which is a contrast to CS by donor-excitation, taking place via the LUMO of the bridge (Figure 2). As CS via the excited state of C_{60} ($^{1}C_{60}$*), two routes can be considered; one is the direct excitation case and another is the indirect excitation case as shown in Figure 31. In the indirect case, immediately after donor excitation, EnT takes place to C_{60}, generating $^{1}C_{60}$*, from which CS takes place.[54,55]

Since bisbiphenylaniline (*N*,*N*-bis(biphenylyl)aniline; BBA) is a very good electron donor with respect to $^{1}C_{60}$*, several studies of BBA–spacer–C_{60} molecules have been reported as shown in Figure 32.[56,57] One of the merits of the study of BBA–spacer–C_{60} molecules is the sharp and intense absorption

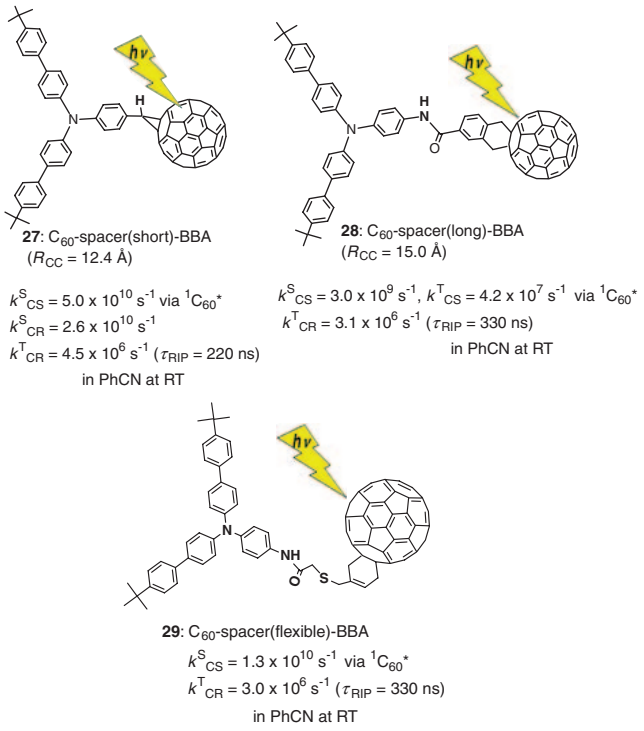

Figure 32. Rates of BBA–spacer–C_{60} molecules (compounds **27**, **28**, and **29**).[56–58]

band at 900 nm of the radical cation of BBA moiety. Thus, their transient absorption studies gave quite highly quantitative rate parameters for the CS process via the $^1C_{60}$* moiety and CR from BBA$^{\bullet+}$–spacer–$C_{60}^{\bullet-}$. The observed k^S_{CS} values decrease with the length of the spacer; from $R_{CC} = 13$ Å for BBA–spacer(short)–C_{60} (compound **27**) to $R_{CC} = 15$ Å for BBA–spacer(long)–C_{60} (compound **28**), the k^S_{CS} values decrease by 1/10. However, the k^T_{CR} values decrease only slightly from 4.5×10^6 to $3.1 \times 10^6\,s^{-1}$, suggesting that the rates of CR are not controlled only by the R_{CC} values, when the R_{CC} values are small. In the case of flexible spacer (compound **29**), in which the BBA moiety and the C_{60} sphere have a chance to approach closely, large k^S_{CS} values up to $1 \times 10^{10}\,s^{-1}$ were observed, but the k^T_{CR} value was similar to those of the rigid spacers (compounds **27** and **28**).[58]

As for short molecular wires, a comparison between the phenylvinyl (PV) linkage (compound **30**) and the phenylethynyl (abbreviated as phenylacetyl and PA) linkage (compound **31**) is possible for ferrocene (Fc) as electron donor (Figure 33).[59,60] The R_{CC} value for (Fc–PA)$_2$–C_{60} is larger than that of (Fc–PV)$_2$–C_{60}; thus, the observed k^S_{CS} values decrease with the length of the bridges. However, the tendency of the k^T_{CR} value is opposite to this trend, suggesting higher electron-transferring ability of the PA linkage than the PV linkage in CR.

For longer molecular wires, the most typical example for long distance CS via the excited state of C_{60} was reported for oligophenylenevinylene molecular wires with extended-TTF as electron donor (compounds **32**–**34** in Figure 34) by Giacalone et al.[61,62] The k^S_{CS} values fall in a very narrow range ((2.4–3.5) $\times 10^9\,s^{-1}$ in THF at RT) with a large change of the R_{CC} from 21 (compound **32**) to 41 Å (compound **34**). Therefore,

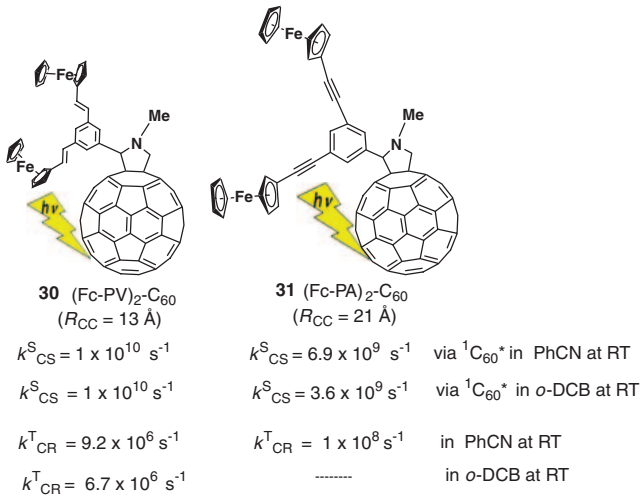

Figure 33. Rates of (Fc–PV)$_2$–C_{60} (compound **30**) and (Fc–PA)$_2$–C_{60} (compound **31**).[59,60]

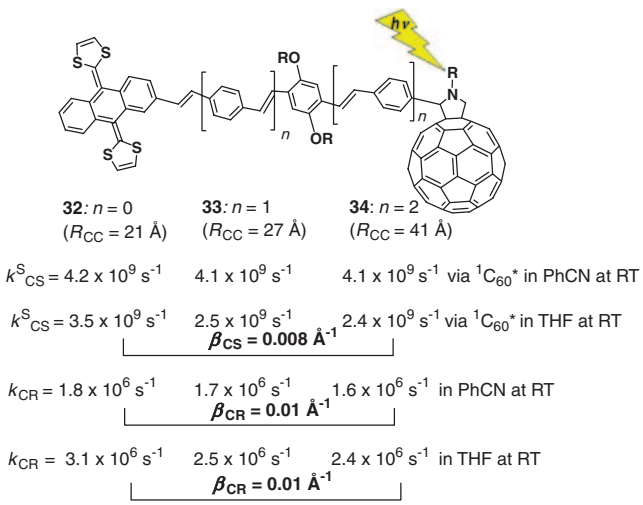

Figure 34. Rate constants of extended-TTF–oligophenylenevinylene–C_{60} (compounds **32**, **33**, and **34**).[61,62]

the β_{CS} value was calculated to be 0.008 Å^{-1}, which is smaller than the β_{CS} (0.02 Å^{-1}) of the *n*TV units (in Figure 27).[48] Such a small β_{CS} value indicates that CS via $^1C_{60}$* takes place even for R_{CC} = ca. 80 Å until the ISC of $^1C_{60}$* ($8 \times 10^8\,s^{-1}$) exceeds the k^S_{CS} value at $R_{CC} = 80$ Å. This β_{CS} value is smaller than that for the donor excitation of ZnP–oligophenylenevinylene–C_{60} ($\beta_{CS} = 0.03$ Å^{-1} in THF at RT in Figure 18). Since the k^S_{CS} values of extended-TTF–oligophenylenevinylene–C_{60} are also in the same range as those of ZnP–oligophenylenevinylene–C_{60}, the main factor determining the β_{CS} values may be the higher π-electron delocalization along the HOMO of the oligophenylenevinylene than that of the LUMO. In Figure 19, the LUMO and HOMO of the oligophenylenevinylenes are shown; the number of nodes may be related to this property, since the number in the HOMO is less than that in the LUMO.

In the case of CR for extended-TTF–oligophenylenevinylene–C_{60}, the β_{CR} value was determined to be 0.01 Å^{-1},[61,62] which is slightly smaller than that of ZnP–oligophenylenevinylene–C_{60} ($\beta_{CR} = 0.02$–0.04 Å^{-1} in THF and PhCN, see Figure 18). Between the two possible routes of CR in

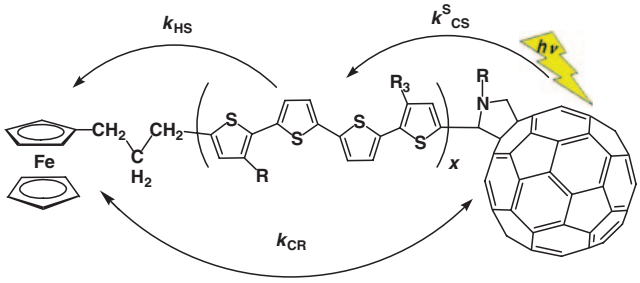

Fc-$(CH_2)_3$-nT-C_{60} (n = 4, 8, 12 x = 1, 2, 3)

	35: n = 4	**36**: n = 8	**37**: n = 12
	(R_{CC} = 22.8 Å)	(R_{CC} = 35.7 Å)	(R_{CC} = 50.9 Å)
k^S_{CS} =	8.1 x 10^{11} s^{-1}	4.5 x 10^{11} s^{-1}	2.8 x 10^{11} s^{-1}
	β_{CS} = 0.18 Å^{-1} via C_{60}* in PhCN at RT		
k_{HS} =	3.8 x 10^{10} s^{-1}	3.1 x 10^{10} s^{-1}	1.3 x 10^{10} s^{-1}
k_{CR} =	4.6 x 10^{7} s^{-1}	4.2 x 10^{6} s^{-1}	3.0 x 10^{6} s^{-1}

in PhCN at RT

Figure 35. Rate constants of Fc–$(CH_2)_3$–nT–C_{60} (compounds **35**, **36**, and **37**).[63]

Figure 3, the CR-1 route may be more probable than the CR-1′ route, because of the direct connection of the vinylene unit with the extended-TTF moiety. Therefore, ET through the HOMOs of the oligophenylenevinylenes takes place in CR of extended-TTF$^{\bullet+}$–oligophenylenevinylene–$C_{60}^{\bullet-}$. In the case of ZnP$^{\bullet+}$–oligophenylenevinylene–$C_{60}^{\bullet-}$ (Figure 18), the energy level of the LUMO of oligophenylenevinylene is usually higher than that of the half-filled LUMO of ZnP$^{\bullet+}$; thus, the CR-1′ route is difficult, whereas ET from the HOMO of the oligophenylenevinylene bridge to the half-vacant HOMO of ZnP$^{\bullet+}$ (CR-1 route) is more probable. Thus, the both β_{CS} values reflect the properties of the HOMO of the oligophenylenevinylene bridge, giving similar β_{CR} values.

Two types of C_{60} derivatives have been reported for ferrocene (Fc) as an electron-donor connected with oligothiophene molecular wires. One type is Fc–$(CH_2)_3$–nT–C_{60} (compounds **35**, **36**, and **37**), in which the Fc and nT moieties are connected via –$(CH_2)_3$– to prevent direct π-conjugation between them (Figure 35).[63] The other type is directly connected Fc–nT–C_{60} (compounds **38**, **39**, and **40**) as shown in Figure 36.[63]

By combination of the fluorescence decays and transient absorption measurements, stepwise CS via $^1C_{60}$* is revealed. The first step is CS via $^1C_{60}$* to generate Fc–$(CH_2)_3$–nT$^{\bullet+}$–$C_{60}^{\bullet-}$ (k^S_{CS} in Figure 35); the second step is the hole-shift from Fc–$(CH_2)_3$–nT$^{\bullet+}$–$C_{60}^{\bullet-}$ to Fc$^{\bullet+}$–$(CH_2)_3$–nT–$C_{60}^{\bullet-}$ (k_{HS} in Figure 35). With an increase in the nT units, the k^S_{CS} values decrease; from the electron-donor ability, an opposite tendency would be anticipated only by the energetic considerations. Thus, these decreases in the k^S_{CS} values suggest that a hole is generated at the center of the nT$^{\bullet+}$ unit, which is also distance dependent. Similarly, the k_{HS} values increase with an increase in the nT units, which is a reasonable trend on the basis of increasing stability of the nT$^{\bullet+}$ units with increase of n, in addition to the distance dependence of the hole position.

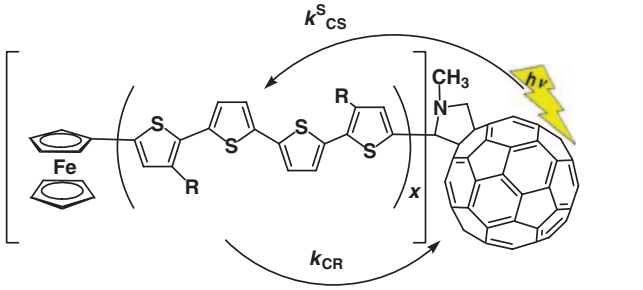

Fc-nT-C_{60} (n = 4, 8, 12 x = 1, 2, 3)

38: n = 4	**39**: n = 8	**40**: n = 12
k^S_{CS} > 1 x 10^{11} s^{-1}	1 x 10^{11} s^{-1}	1 x 10^{11} s^{-1} via $^1C_{60}$*
k_{CR} = 1.2 x 10^{10} s^{-1}	3.7 x 10^{8} s^{-1}	2.0 x 10^{7} s^{-1}

in PhCN at RT

Figure 36. Rate constants of Fc–nT–C_{60} (compounds **38**, **39**, and **40**).[63]

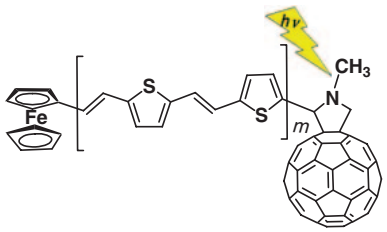

41: m = 1 (R_{CC} = 11.4 Å)	**42**: m = 2 (R_{CC} = 14.4 Å)
k^S_{CS} = 6.2 x 10^9 s^{-1} via $^1C_{60}$*	k^S_{CS} = 1.7 x 10^{11} s^{-1} via $^1C_{60}$*
k_{CR} > 2 x 10^6 s^{-1}	k_{CR} = 2 x 10^8 s^{-1}

in PhCN at RT

Figure 37. Rate constants of Fc–nTV–C_{60} (compounds **41**: $n = 2$ and **42**: $n = 4$).[64]

As for the direct CR, a drastic decrease in the k_{CR} values was observed from Fc$^{\bullet+}$–$(CH_2)_3$–4T–$C_{60}^{\bullet-}$ to Fc$^{\bullet+}$–$(CH_2)_3$–8T–$C_{60}^{\bullet-}$, suggesting direct CR for 4T, whereas for 8T and 12T, stepwise CR via Fc–$(CH_2)_3$–nT$^{\bullet+}$–$C_{60}^{\bullet-}$ would be in effect.

In the directly connected case (Fc–nT–C_{60}; compounds **38**, **39**, and **40**), fast CS via $^1C_{60}$* generating (Fc–nT)$^{\bullet+}$–$C_{60}^{\bullet-}$ was observed ($k^S_{CS} > 10^{11}\,s^{-1}$) as confirmed by femto-second transient absorption spectra.[62] The k_{CR} values for (Fc–nT)$^{\bullet+}$–$C_{60}^{\bullet-}$ showed drastic decrease by 1/500 from $10^{10}\,s^{-1}$ for (Fc–4T)$^{\bullet+}$–$C_{60}^{\bullet-}$ to $2 \times 10^7\,s^{-1}$ for (Fc–12T)$^{\bullet+}$–$C_{60}^{\bullet-}$ with a change of R_{CC} = ca. 30 Å as listed in Figure 36. Such a big change in the k_{CR} values suggests that the center of the radical cation (hole) is localized on the middle of the Fc–nT moiety and CR occurs through the remaining nT moieties between the hole center and $C_{60}^{\bullet-}$.

More recently, nTV bridges have been used as connectors of Fc and C_{60} as shown in Figure 37 (compounds **41** and **42**).[64] For Fc–2TV–C_{60} (compound **41**), the CS state via $^1C_{60}$* was confirmed as (Fc–2TV)$^{\bullet+}$–$C_{60}^{\bullet-}$ by the transient absorption spectra, whereas for Fc–4TV–C_{60} (compound **42**), the CS state via $^1C_{60}$* was confirmed as Fc$^{\bullet+}$–4TV–$C_{60}^{\bullet-}$. Thus, the k^S_{CS} values cannot be directly compared. As for the k_{CR} values, an

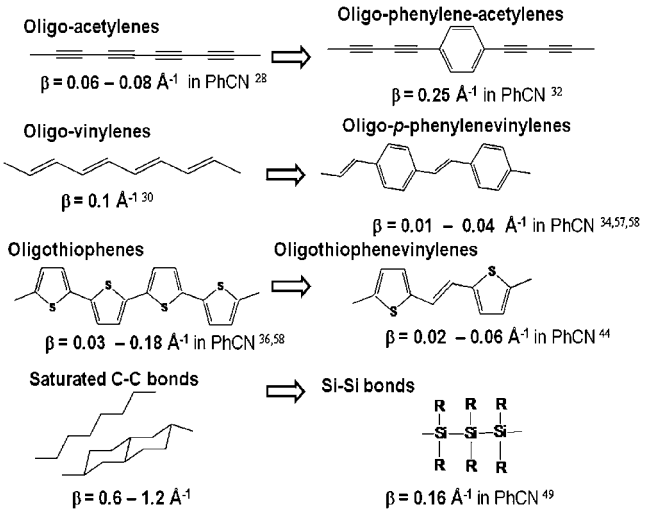

Figure 38. Damping factors (β_{ET}) of some bridges; the references are cited in the text.

opposite tendency to that expected from the distance dependence was observed, although a direct comparison of the CR rates between $(Fc–2TV)^{\bullet+}–C_{60}^{\bullet-}$ and $Fc^{\bullet+}–4TV–C_{60}^{\bullet-}$ is difficult. From the large k^S_{CS} and k_{CR} values for Fc–4TV–C_{60}, it can be presumed that the electron conductivity through the HOMO of the 4TV bridge is very high.

Conclusion

In the photoinduced events of the porphyrin–bridge–fullerene triads, porphyrins act as photosensitizing electron donors to the ground state of C_{60} acting as an electron acceptor over the bridges. In such case, the LUMO of the bridges can be used as a mediator of an electron via super-exchange and hopping mechanisms, depending on their relative MO energy levels. The damping factors have been evaluated for both charge separation and charge recombination, in which the latter process usually uses the HOMO of the bridges. Among the π-conjugated bridges, the oligothiophenes gave the smallest damping factor affording long distance charge separation.

In the case of fullerene excitation, charge separation via the excited state of fullerene acceptor usually takes place via the HOMO of the bridges, thus the damping factors are compared with those of the porphyrin excitation case.

The observed damping factors of the molecular wires are summarized in Figure 38. Although the damping factors (β_{ET}) depend on solvent polarity and also on the donor and acceptor pair, the π-conjugation of the bridges is the main factor. From MO considerations, it would be expected that the CS through the LUMO of the bridges may give different β_{ET} from the CR through the HOMO, however appreciable differences were not observed between the β_{CS} and β_{CR} values.

Compared with the β_{ET} values of the oligoacetylene bridges, the β_{ET} values of the oligophenyleneacetylene bridges are large, indicating that the phenyl group between the acetylene units acts as a resisting element for the electron and hole conducting property of the oligoacetylene bridges. On the other hand, an opposite tendency was observed for the vinylene bridges and phenylenevinylene bridges. It can be pointed out that the shapes of MOs of the repeating units of bridges are important to control the β_{ET} values, in addition to the energy differences influencing the super-exchange mechanism and hopping mechanism.

The authors would like to acknowledge Drs. Y. Araki, A. S. D. Sandanayaka, M. Sasaki, and M. El-Khouly of Tohoku University, Professor K. Tamao and Dr. T. Nakamura of RIKEN, Professors K. Tashiro, H. Tsuji, and T. Aida of the University of Tokyo, Professor T. Takata of Tokyo Institute of Technology, Professor H. Imahori of Kyoto University, Professors M. Fujitsuka, S. Fukuzumi, and Y. Aso of Osaka University, Professors T. Otsubo and K. Takimiya of Hiroshima University, Professor F. D'Souza of Wichita University (USA), Professor F. Langa of University of Castilla-la Mancha (Spain), and Mr. S. Shirai and the CAE Promotion Office of Toyota Central R&D Labs., Inc.

References

1 *Photoinduced Electron Transfer*, ed. by M. A. Fox, M. Chanon, Elsevier, Amsterdam, **1988**, Part D.

2 *Fundamentals of Photoinduced Electron Transfer*, ed. by G. J. Kavarnos, VCH Publisher, New York, **1993**.

3 O. Ito, *Res. Chem. Intermed.* **1997**, *23*, 389.

4 *Electron Transfer in Chemistry*, ed. by V. Balzani, Wiley-VCH, Weinheim, **2001**.

5 P. J. Bracher, D. Schuster, in *Fullerenes: from Synthesis to Optoelectronic Properties,* ed. by D. M. Guldi, N. Martín, Kluwer Academic Publishers, New York, **2002**.

6 A. S. D. Sandanayaka, H. Sasabe, Y. Araki, N. Kihara, Y. Furusho, T. Takata, O. Ito, *Aust. J. Chem.* **2006**, *59*, 186.

7 M. R. Wasielewski, D. G. Johnson, W. A. Svec, K. M. Kersey, D. E. Cragg, D. W. Minsek, in *Photochemical Energy Conversion*, ed. by J. R. Norris, D. Meisel, Elsevier, Amsterdam, **1989**.

8 T. Okada, T. Fujita, M. Kubota, S. Masaki, N. Mataga, R. Ide, Y. Sakata, S. Misumi, *Chem. Phys. Lett.* **1972**, *14*, 563.

9 S. Masaki, T. Okada, N. Mataga, Y. Sakata, S. Misumi, *Bull. Chem. Soc. Jpn.* **1976**, *49*, 1277.

10 T. Okada, M. Migita, N. Mataga, Y. Sakata, S. Misumi, *J. Am. Chem. Soc.* **1981**, *103*, 4715.

11 M. Migita, T. Okada, N. Mataga, S. Nishitani, N. Kurata, Y. Sakata, S. Misumi, *Chem. Phys. Lett.* **1981**, *84*, 263.

12 N. S. Sariciftci, L. Smilowitz, A. J. Heeger, F. Wudl, *Science* **1992**, *258*, 1474.

13 K. Yoshino, X. H. Yin, S. Morita, T. Kawai, A. A. Zakhidov, *Solid State Commun.* **1993**, *85*, 85.

14 V. May, O. Kühn, *Charge and Energy Transfer Dynamics in Molecular Systems*, 2nd ed., Wiley-VCH, Weinheim, **2004**.

15 W. B. Davis, W. A. Svec, M. A. Rather, M. R. Wasielewski, *Nature* **1998**, *396*, 60.

16 B. G. Maiya, T. Ramasarma, *Curr. Sci.* **2001**, *80*, 1523.

17 H. Imahori, K. Tamaki, D. M. Guldi, C. Luo, M. Fujitsuka, O. Ito, Y. Sakata, S. Fukuzumi, *J. Am. Chem. Soc.* **2001**, *123*, 2607.

18 F. D'Souza, G. R. Deviprasad, M. E. Zandler, M. E. El-Khouly, M. Fujitsuka, O. Ito, *J. Phys. Chem. B* **2002**, *106*, 4952.

19 F. D'Souza, P. M. Smith, M. E. Zandler, A. L. McCarty, M. J. Kullman, M. Itou, Y. Araki, O. Ito, *J. Am. Chem. Soc. B* **2004**, *126*, 7898.

20 D. M. Guldi, P. V. Kamat, in *Fullerenes, Chemistry,*

Physics and Technology, ed. by K. M. Kadish, R. S. Ruoff, Wiley-Interscience, New York, **2000**, pp. 225–281.

21 M. Fujitsuka, O. Ito, in *Handbook of Photochemistry and Photobiology,* ed. by H. Nalwa, American Science Publisher, CA, **2003**, Vol. 2.

22 H. Imahori, K. Hagiwara, T. Akiyama, M. Aoki, S. Taniguchi, T. Okada, M. Shirakawa, Y. Sakata, *Chem. Phys. Lett.* **1996**, *263*, 545.

23 M. E. El-Khouly, O. Ito, P. M. Smith, F. D'Souza, *J. Photochem. Photobiol., C* **2004**, *5*, 79.

24 N. V. Tkachenko, H. Lemmetyinen, J. Sonoda, K. Ohkubo, T. Sato, H. Imahori, S. Fukuzumi, *J. Phys. Chem. A* **2003**, *107*, 8834.

25 For some zinc porphyrin–C_{60} dyads with short bridge, see also: K. Yamanaka, M.S. Thesis, Tohoku University, **2003**.

26 H. Imahori, M. E. El-Khouly, M. Fujitsuka, O. Ito, Y. Sakata, S. Fukuzumi, *J. Phys. Chem. A* **2001**, *105*, 325.

27 A. S. D. Sandanayaka, K. Ikeshita, Y. Araki, N. Kihara, Y. Furusho, T. Takata, O. Ito, *J. Mater. Chem.* **2005**, *15*, 2276.

28 A. S. D. Sandanayaka, K. Ikeshita, N. Watanabe, Y. Araki, Y. Furusho, N. Kihara, T. Takata, O. Ito, *Bull. Chem. Soc. Jpn.* **2005**, *78*, 1008.

29 J. W. Verhoeven, *J. Photochem. Photobiol., C* **2006**, *7*, 40.

30 H. Imahori, H. Yamada, D. M. Guldi, Y. Endo, A. Shimomura, S. Kundu, K. Yamada, T. Okada, Y. Sakata, S. Fukuzumi, *Angew. Chem., Int. Ed.* **2002**, *41*, 2344.

31 S. A. Vail, D. I. Schuster, D. M. Guldi, M. Isosomppi, N. Tkachenko, H. Lemmetyinen, A. Palkar, L. Echegoyen, X. Chen, J. Z. H. Zhang, *J. Phys. Chem. B* **2006**, *110*, 14155.

32 S. A. Vail, P. J. Krawczuk, D. M. Guldi, A. Palkar, L. Echegoyen, J. P. Tomé, M. A. Fazio, D. I. Schuster, *Chem.—Eur. J.* **2005**, *11*, 3375.

33 K. Yamanaka, M. Fujitsuka, Y. Araki, K. Tashiro, A. Sato, T. Yuzawa, T. Aida, *J. Porphyrins Phthalocyanines* **2007**, *11*, 397.

34 A. Osuka, N. Tanabe, S. Kawabata, I. Yamazaki, Y. Nishimura, *J. Org. Chem.* **1995**, *60*, 7177.

35 These MO calculation data were kindly offered by Dr. Y. Araki of Tohoku University and Mr. S. Shirai of Toyota Central R&D Labs., to whom the authors are thankful.

36 K. Tashiro, A. Sato, T. Yuzawa, T. Aida, K. Yamanaka, M. Fujitsuka, O. Ito, *Chem. Lett.* **2006**, *35*, 518.

37 M. Quintiliani, A. Kahnt, T. Wölfle, W. Hieringer, P. Vázquez, A. Görling, D. M. Guldi, T. Torres, *Chem.—Eur. J.* **2008**, *14*, 3765.

38 G. de la Torre, F. Giacalone, J. L. Segura, N. Martín, D. M. Guldi, *Chem.—Eur. J.* **2005**, *11*, 1267.

39 H. D. Sikes, J. F. Smalley, S. P. Dudek, A. R. Cook, M. D. Newton, C. E. D. Chidsey, S. W. Feldberg, *Science* **2001**, *291*, 1519.

40 T. Nakamura, M. Fujitsuka, Y. Araki, O. Ito, J. Ikemoto, K. Takimiya, Y. Aso, T. Otsubo, *J. Phys. Chem. B* **2004**, *108*, 10700.

41 T. Nakamura, J. Ikemoto, M. Fujitsuka, Y. Araki, O. Ito, K. Takimiya, Y. Aso, T. Otsubo, *J. Phys. Chem. B* **2005**, *109*, 14365.

42 T. Nakamura, Y. Araki, O. Ito, K. Takimiya, T. Otsubo, *J. Phys. Chem. A* **2008**, *112*, 1125.

43 Some of these MOs are cited from supporting information of Ref. 40, to which additional data were calculated by Drs. T. Nakamura and Y. Araki. The authors are thankful to them.

44 M. Fujitsuka, O. Ito, T. Yamashiro, Y. Aso, T. Otsubo, *J. Phys. Chem. A* **2000**, *104*, 4876.

45 M. Fujitsuka, K. Matsumoto, O. Ito, T. Yamashiro, Y. Aso, T. Otsubo, *Res. Chem. Intermed.* **2001**, *27*, 73.

46 T. Oike, T. Kurata, K. Takimiya, T. Otsubo, Y. Aso, H. Zhang, Y. Araki, O. Ito, *J. Am. Chem. Soc.* **2005**, *127*, 15372.

47 O. Ito, H. Zhang, T. Oike, T. Kurata, K. Takimiya, T. Otsubo, Y. Aso, Y. Araki, *ECS Trans.* **2006**, *2*, 51.

48 F. Oswald, D.-M. S. Islam, Y. Araki, V. Troiani, R. Caballero, P. de la Cruz, O. Ito, F. Langa, *Chem. Commun.* **2007**, 4498.

49 Including $n = 3$ and 8 for ZnP–*n*TV–C_{60}, similarly small β_{CS} was evaluated: F. Oswald, D.-M. S. Islam, M. E. El-Khouly, Y. Araki, R. Caballero, P. de la Cruz, O. Ito, F. Langa, unpublished data.

50 J. J. Apperloo, C. Martineau, P. A. van Hal, J. Roncali, R. A. J. Janssen, *J. Phys. Chem. A* **2002**, *106*, 21.

51 H. Tsuji, M. Sasaki, Y. Shibano, M. Toganoh, T. Kataoka, Y. Araki, K. Tamao, O. Ito, *Bull. Chem. Soc. Jpn.* **2006**, *79*, 1338.

52 Some of these MOs are cited from supporting information of Ref. 51, to which additional data were calculated by Drs. M. Sasaki, Y. Araki, and H. Tsuji. The authors are thankful to them.

53 M. Sasaki, Y. Shibano, H. Tsuji, Y. Araki, K. Tamao, O. Ito, *J. Phys. Chem. A* **2007**, *111*, 2973.

54 Y. Araki, O. Ito, in *Handbook of Organic Electronics and Photonics*, ed. by H. S. Nalwa, American Scientific Publishers, California, **2008**, Vol. 2, Chap. 12, pp. 473–513.

55 Y. Araki, O. Ito, *J. Photochem. Photobiol., C* **2008**, *9*, 93.

56 S. Komamine, M. Fujitsuka, O. Ito, K. Moriwaki, T. Miyata, T. Ohno, *J. Phys. Chem. A* **2000**, *104*, 11497.

57 G. A. Rajkumar, A. S. D. Sandanayaka, K. Ikeshita, M. Itou, Y. Araki, Y. Furusho, N. Kihara, O. Ito, T. Takata, *J. Phys. Chem. A* **2005**, *109*, 2428.

58 A. S. D. Sandanayaka, K. Ikeshita, G. A. Rajkumar, Y. Furusho, Y. Araki, T. Takata, O. Ito, *J. Phys. Chem. A* **2005**, *109*, 8088.

59 L. Perez, M. E. El-Khouly, P. de la Cruz, Y. Araki, O. Ito, F. Langa, *Eur. J. Org. Chem.* **2007**, 2175.

60 L. Pérez, D.-M. S. Islam, Y. Araki, P. de la Cruz, F. Cardinali, O. Ito, F. Langa, *Eur. J. Org. Chem.* **2008**, 3535.

61 F. Giacalone, J. L. Segura, N. Martín, D. M. Guldi, *J. Am. Chem. Soc.* **2004**, *126*, 5340.

62 F. Giacalone, J. L. Segura, N. Martín, J. Ramey, D. M. Guldi, *Chem.—Eur. J.* **2005**, *11*, 4819.

63 T. Nakamura, H. Kanato, Y. Araki, O. Ito, K. Takimiya, T. Otsubo, Y. Aso, *J. Phys. Chem. A* **2006**, *110*, 3471.

64 F. Oswald, D.-M. S. Islam, Y. Araki, V. Troiani, P. de la Cruz, A. Moreno, O. Ito, F. Langa, *Chem.—Eur. J.* **2007**, *13*, 3924.

Osamu Ito was born in 1943 in Koga city, Ibaraki. He graduated from the Department of Chemistry of Tohoku University with a Ph.D. in 1973. His academic career began at Tohoku University in Sendai (Japan) as an associate researcher (1973–1983), as an associate professor (1984–1992) and as a full professor (1993–2007). In 2007, he retired from Tohoku University as a Professor Emeritus. His main research is photochemistry based on flash photolysis methods for probing free radical reactions and electron-transfer reactions. He expanded his research interests to fullerenes and nanocarbon materials using near-IR transient absorption spectrophotometry. He was a recipient of the Mitsubishi Foundation Award in 2004, and the Japanese Photochemistry Association Lectureship Award in 2006.

Ken-ichi Yamanaka was born in Chiba in 1977. He received a B.S. degree from Yokohama National University under the direction of Prof. M. Yagi in 2001 and then received an M.S. degree from Tohoku University under the direction of Prof. O. Ito in 2003. He started his career at Asahi Glass Co., Ltd. and then moved to Toyota Central R&D Labs., Inc. in 2004. He also joined CREST-JST promoted by Dr. S. Inagaki in 2006. His present research interests include the excited-state dynamics of optically-opaque photo-functionalized materials using time-resolved spectroscopy, especially transient diffuse reflectance, fluorescence up-conversion, and time-correlated single photon counting techniques, in the wide time regions from femtosecond to millisecond and wide wavelength regions in the UV, vis, and near-IR regions.